Observation of a new Ξ_b^0 state

R. Aaij *et al.*[*]
(LHCb Collaboration)

(Received 28 October 2020; accepted 23 November 2020; published 6 January 2021)

Using a proton-proton collision data sample collected by the LHCb experiment, corresponding to an integrated luminosity of 8.5 fb^{-1}, the observation of a new excited Ξ_b^0 resonance decaying to the $\Xi_b^-\pi^+$ final state is presented. The state, referred to as $\Xi_b(6227)^0$, has a measured mass and natural width of $m(\Xi_b(6227)^0) = 6227.1^{+1.4}_{-1.5} \pm 0.5$ MeV and $\Gamma(\Xi_b(6227)^0) = 18.6^{+5.0}_{-4.1} \pm 1.4$ MeV, where the uncertainties are statistical and systematic. The production rate of the $\Xi_b(6227)^0$ state relative to that of the Ξ_b^- baryon in the kinematic region $2 < \eta < 5$ and $p_{\mathrm{T}} < 30$ GeV is measured to be $\frac{f_{\Xi_b(6227)^0}}{f_{\Xi_b^-}} \mathcal{B}(\Xi_b(6227)^0 \to \Xi_b^-\pi^+) = 0.045 \pm 0.008 \pm 0.004$, where $\mathcal{B}(\Xi_b(6227)^0 \to \Xi_b^-\pi^+)$ is the branching fraction of the decay, and $f_{\Xi_b(6227)^0}$ and $f_{\Xi_b^-}$ represent fragmentation fractions. Improved measurements of the mass and natural width of the previously observed $\Xi_b(6227)^-$ state, along with the mass of the Ξ_b^- baryon, are also reported. Both measurements are significantly more precise than, and consistent with, previously reported values.

DOI: 10.1103/PhysRevD.103.012004

I. INTRODUCTION

In the constituent quark model [1,2], baryonic states form multiplets according to the symmetry of their flavor, spin and spatial wave functions. The masses, natural widths and decay modes of these states give insight into their internal structure [3]. The Ξ_b^0 and Ξ_b^- states form an isodoublet of bsq bound states, where q is a u or d quark, respectively. Three such isodoublets, which are neither radially nor orbitally excited, should exist [4], and include the Ξ_b state with spin $j_{qs} = 0$ and $J^P = (1/2)^+$, the Ξ_b' with $j_{qs} = 1$ and $J^P = (1/2)^+$, and the Ξ_b^* with $j_{qs} = 1$ and $J^P = (3/2)^+$. Here, j_{qs} is the spin of the light diquark system qs, and J^P represents the spin and parity of the state. Three of the four $j_{qs} = 1$ states have been observed through their decays to $\Xi_b^0\pi^-$ and $\Xi_b^-\pi^+$ final states [5–7].

Beyond these lowest-lying Ξ_b states, a spectrum of heavier states is expected [8–22], where there are either radial or orbital excitations among the constituent quarks. Recently, peaks in the $\Lambda_b^0 K^-$ and $\Xi_b^0\pi^-$ invariant-mass spectra corresponding to a mass of 6227 MeV[1] have been reported [23], and subsequent constituent quark model [24–30] and quark-diquark [31–34] analyses show that this state is consistent with a P-wave Ξ_b^- excitation. Alternative investigations argue that the state could also be wholly or partially molecular in nature [35–38]. More information on the observed states, or observation of additional excited beauty-baryon states, will provide additional input for these theoretical investigations.

In this article, the observation of a new beauty-baryon resonance, referred to as $\Xi_b(6227)^0$, is reported using samples of proton-proton (pp) collision data collected with the LHCb experiment at center-of-mass energies of $\sqrt{s} = 7$, 8 TeV (Run 1) and 13 TeV (Run 2), corresponding to integrated luminosities of 1.0, 2.0 and 5.5 fb^{-1}, respectively. The resonance is seen through its decay to the $\Xi_b^-\pi^+$ final state, where the Ξ_b^- baryon is reconstructed in the fully hadronic decay channels $\Xi_c^0\pi^-$ and $\Xi_c^0\pi^-\pi^+\pi^-$, with $\Xi_c^0 \to pK^-K^-\pi^+$. Charge-conjugate processes are implicitly included throughout this paper.

Using the 13 TeV data, the production rate of the $\Xi_b(6227)^0$ state is measured relative to that of the Ξ_b^- baryon as

$$R(\Xi_b^-\pi^+) \equiv \frac{f_{\Xi_b(6227)^0}}{f_{\Xi_b^-}} \mathcal{B}(\Xi_b(6227)^0 \to \Xi_b^-\pi^+). \quad (1)$$

Here, $f_{\Xi_b(6227)^0}$ and $f_{\Xi_b^-}$ are the fragmentation fractions for $b \to \Xi_b(6227)^0$ and $b \to \Xi_b^-$, which include contributions from the decays of higher-mass b-hadrons, and $\mathcal{B}(\Xi_b(6227)^0 \to \Xi_b^-\pi^+)$ is the branching fraction of the decay.

The same pp collision data set is used to improve the precision on the mass and width of the recently observed $\Xi_b(6227)^-$ state [23] using the $\Xi_b(6227)^- \to \Lambda_b^0 K^-$ decay

[*]Full author list given at the end of the article.
[1]Natural units with $c = 1$ are used throughout this paper.

mode. The analysis presented here benefits greatly from the larger data sample, but also by using both $\Lambda_b^0 \to \Lambda_c^+\pi^-$ and $\Lambda_b^0 \to \Lambda_c^+\pi^-\pi^+\pi^-$ decays, leading to about a four-fold increase in the Λ_b^0 yield over that which was used in Ref. [23].

Lastly, with the large samples of Ξ_b^- and Λ_b^0 decays obtained in this analysis, the most precise measurement of the Ξ_b^- mass to date is presented. The Ξ_b^- mass obtained in this analysis is then used to obtain the mass of the $\Xi_b(6227)^0$ resonance.

II. DETECTOR AND SIMULATION

The LHCb detector [39,40] is a single-arm forward spectrometer covering the pseudorapidity range $2 < \eta < 5$, designed for the study of particles containing b or c quarks. The detector includes a high-precision tracking system consisting of a silicon-strip vertex detector surrounding the pp interaction region, a large-area silicon-strip detector located upstream of a dipole magnet with a bending power of about 4 Tm, and three stations of silicon-strip detectors and straw drift tubes placed downstream of the magnet. The tracking system provides a measurement of the momentum, p, of charged particles with a relative uncertainty that varies from 0.5% at low momentum to 1.0% at 200 GeV. The minimum distance of a track to a primary vertex (PV), the impact parameter (IP), is measured with a resolution of $(15 + 29/p_{\mathrm{T}})$ μm, where p_{T} is the component of the momentum transverse to the beam, in GeV. Different types of charged hadrons are distinguished using information from two ring-imaging Cherenkov detectors. Photons, electrons and hadrons are identified by a calorimeter system consisting of scintillating-pad and preshower detectors, an electromagnetic and a hadronic calorimeter. Muons are identified by a system composed of alternating layers of iron and multiwire proportional chambers. The online event selection is performed by a trigger which consists of a hardware stage, based on information from the calorimeter and muon systems, followed by a software stage, which applies a full event reconstruction.

Simulation is required to model the effects of the detector acceptance and the imposed selection requirements. It is also used to determine the expected invariant-mass resolution. In the simulation, pp collisions are generated using PYTHIA [41] with a specific LHCb configuration [42]. Decays of unstable particles are described by EvtGen [43], in which final-state radiation is generated using PHOTOS [44]. The interaction of the generated particles with the detector, and its response, are implemented using the GEANT4 toolkit [45] as described in Ref. [46].

To improve the agreement of the simulation with the data in modeling the kinematics of beauty baryons within the acceptance of the LHCb detector, the simulated beauty-baryon momentum components, p_{T} and p_z, are transformed to match the distributions obtained from background-subtracted data [47]. Here, p_z is the momentum component along the beam axis. In particular, the p_{T} and p_z are transformed according to

$$p_{\mathrm{T}} \to p'_{\mathrm{T}} = \exp(\kappa_{\mathrm{T}} \log(p_{\mathrm{T}})),$$
$$p_z \to p'_z = \exp(\kappa_z \log(p_z)). \quad (2)$$

For the Λ_b^0 and Ξ_b^- simulations, the values $\kappa_{\mathrm{T}} = 0.98$ and $\kappa_z = 0.99$ bring the simulated p_{T} and p_z distributions into good agreement with those of the data, while for the $\Xi_b(6227)^0$ and $\Xi_b(6227)^-$ simulations, the values $\kappa_T = 0.99$ and $\kappa_z = 1.0$ are found. Values of κ less than unity indicate that the given momentum component needs to be scaled to lower values to bring the simulation into agreement with the data. In the optimization of specific selections and the determination of selection efficiencies, these tunings are employed, as discussed below.

The particle identification (PID) response of charged hadrons produced in simulated signal decays is obtained from dedicated calibration samples from the data where no PID requirements are imposed [48,49]. The $D^{*+} \to D^0\pi^+$ mode is used for the K^- and π^+ meson PID responses and the $\Lambda_b^0 \to \Lambda_c^+\pi^-$ and $\Lambda \to p\pi^-$ decays are used for the proton PID response. Each final-state signal hadron has its PID response drawn from a three-dimensional probability distribution function that depends on the hadron's p and p_{T}, and the number of reconstructed charged particles in the event.

III. SELECTION REQUIREMENTS

A. Ξ_b^- and Λ_b^0 baryon selections

The Ξ_b^- candidates are reconstructed using the $\Xi_c^0\pi^-$ and $\Xi_c^0\pi^-\pi^+\pi^-$ decay modes, while the Λ_b^0 sample uses the $\Lambda_c^+\pi^-$ and $\Lambda_c^+\pi^-\pi^+\pi^-$ final states. The charm baryons are detected through the decays $\Xi_c^0 \to pK^-K^-\pi^+$ and $\Lambda_c^+ \to pK^-\pi^+$. In what follows, H_b refers to either the Λ_b^0 or Ξ_b^- baryon, and H_c signifies the corresponding charm baryon, Λ_c^+ or Ξ_c^0, according to the above decay sequences.

Charged hadrons used to reconstruct the H_b candidates are required to be significantly detached from all PVs in the event using the quantity χ^2_{IP}, which is the difference in χ^2 of the vertex fit of a given PV when the particle is included or excluded from the fit. Each track is required to have $\chi^2_{\mathrm{IP}} > 4$, which corresponds to an IP that is at least twice as large as the expected IP resolution. Loose PID requirements are also imposed on all the H_b decay products to ensure that they are consistent with the intended decay sequence.

The H_c candidates are required to have a good-quality vertex fit, have significant displacement from all PVs in the event, and satisfy the invariant-mass requirements, $|M(pK^-\pi^+) - m_{\Lambda_c^+}| < 18$ MeV and $|M(pK^-K^-\pi^+) - m_{\Xi_c^0}| < 15$ MeV, corresponding to about three times the mass resolution. Here, and throughout this paper, M represents the invariant mass of the particle(s) indicated

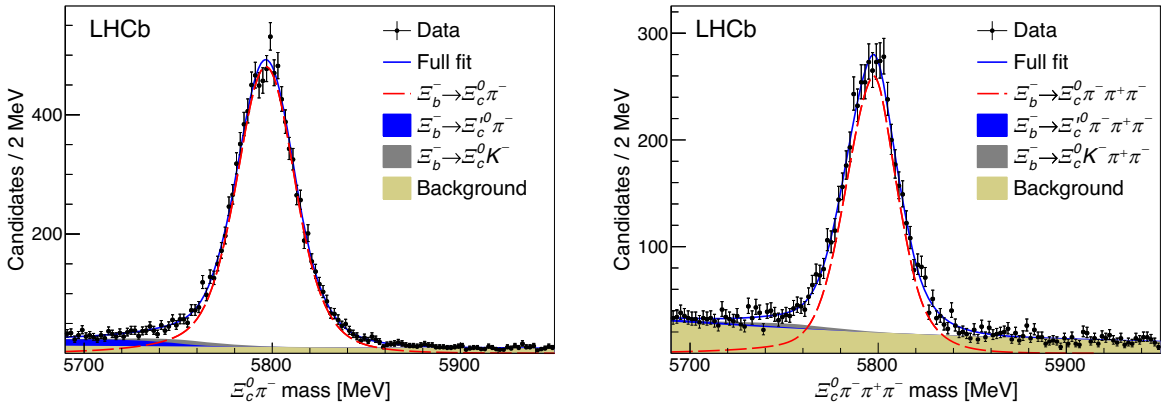

FIG. 1. Invariant-mass spectra for (left) $\Xi_b^- \to \Xi_c^0 \pi^-$ and (right) $\Xi_b^- \to \Xi_c^0 \pi^- \pi^+ \pi^-$ candidates after all selection requirements. Projections of the fits to the data are overlaid.

in parentheses, and m represents the measured mass of the indicated particle, using Ref. [50] for known particles.

One or three charged pions, with total charge -1, are combined with H_c candidates to form the H_b samples. The fitted decay vertex is required to be consistent with a single point in space, evidenced by having good fit quality. To suppress combinatorial background, the H_b decay vertex is required to be significantly displaced from all PVs in the event and have small $\chi^2_{\rm IP}$ to at least one PV. The H_b candidates are assigned to the PV for which $\chi^2_{\rm IP}$ is minimum.

After these selections, clear Ξ_b^- and Λ_b^0 peaks can be seen in the data. The $\Lambda_b^0 \to \Lambda_c^+ \pi^-$ decay mode has an excellent signal-to-background (S/B) ratio, and no further selections are applied. For the $\Xi_b^- \to \Xi_c^0 \pi^-$, $\Xi_b^- \to \Xi_c^0 \pi^- \pi^+ \pi^-$ and $\Lambda_b^0 \to \Lambda_c^+ \pi^- \pi^+ \pi^-$ decays, a boosted decision tree (BDT) discriminant [51–53] is used to further improve the S/B ratio. The set of variables used by the BDT is similar for the three modes. Those common to all three modes include: the χ^2 values of the fitted H_c and H_b decay vertices, the angle between the H_b momentum direction and the vector pointing from the PV to the H_b decay vertex, the H_b and H_c decay times, and for each final-state hadron, p, $p_{\rm T}$, $\chi^2_{\rm IP}$ and a PID response variable. For the $H_b \to H_c \pi^- \pi^+ \pi^-$ modes, three additional variables are included: $M(\pi^- \pi^+ \pi^-)$, the χ^2 of the $\pi^- \pi^+ \pi^-$ vertex fit, and the χ^2 of the vertex separation between the 3π vertex and the associated PV. The BDT is trained using simulated decays for the signal distributions in these variables, and the background distributions are taken from a combination of the H_c or H_b mass sidebands in data. The requirements on the BDT discriminant are chosen based on optimizing the product of signal efficiency and signal purity. The resulting BDT selection requirement is ∼100%, 94% and 93% efficient for $\Xi_b^- \to \Xi_c^0 \pi^-$, $\Xi_b^- \to \Xi_c^0 \pi^- \pi^+ \pi^-$ and $\Lambda_b^0 \to \Lambda_c^+ \pi^- \pi^+ \pi^-$ signal decays, while suppressing the combinatorial background by factors of about 3, 8 and 6, respectively.

In anticipation that the $\Xi_b^- \to \Xi_c^0 \pi^-$ decay mode will be used to measure the relative production rate, $R(\Xi_b^- \pi^+)$, Ξ_b^- candidates are restricted to lie in the kinematic region $p_{\rm T} < 30$ GeV and $2 < \eta < 5$; this selection retains 99.7% of the signal decays.

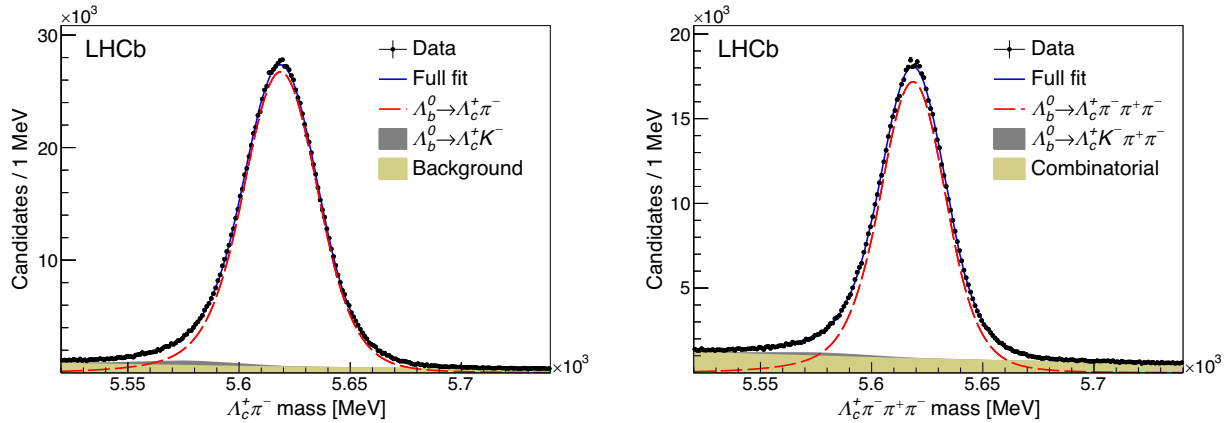

FIG. 2. Invariant-mass spectra for (left) $\Lambda_b^0 \to \Lambda_c^+ \pi^-$ and (right) $\Lambda_b^0 \to \Lambda_c^+ \pi^- \pi^+ \pi^-$ candidates after all selection requirements. Projections of the fits to the data are overlaid.

With all of the selections applied, the resulting Ξ_b^- and Λ_b^0 candidate invariant-mass spectra are shown in Figs. 1 and 2, respectively. The fits, as described below, are overlaid.

B. $\Xi_b(6227)^0$ selection

The $\Xi_b(6227)^0$ candidates are formed by combining a Ξ_b^- candidate with a π^+ meson consistent with coming from the same PV. The $\Xi_b^- \to \Xi_c^0\pi^-$ and $\Xi_b^- \to \Xi_c^0\pi^-\pi^+\pi^-$ candidates are required to have their masses in the intervals $5737 < M(\Xi_c^0\pi^-) < 5847$ MeV and $5750 < M(\Xi_c^0\pi^-\pi^+\pi^-) < 5840$ MeV, respectively, corresponding to about three times the mass resolution about the Ξ_b^- mass [50].

The majority of particles from the PV are pions, and therefore only a loose requirement is applied to the pion PID hypothesis, sufficient to render the contribution from misidentified kaons and protons to be at the few percent level. To suppress background from random π^+ mesons, which tend to have lower p_T than those from b-hadron decays, the selection on the p_T of the π^+ candidate is optimized as follows. The Punzi figure-of-merit [54] $\mathrm{FOM} = \epsilon(p_T)/(\sqrt{N_B(p_T)} + a/2)$ with $a = 5$ is used, where $\epsilon(p_T)$ and $N_B(p_T)$ are the signal efficiency and background yield as a function of the applied π^+ meson p_T requirement. For the signal efficiency, $\epsilon(p_T)$, the π^+ meson p_T is scaled by the ratio p_T'/p_T, as given in Eq. (2). The optimal requirements are $p_T > 700$ MeV and 900 MeV for the $\Xi_b^- \to \Xi_c^0\pi^-$ and $\Xi_b^- \to \Xi_c^0\pi^-\pi^+\pi^-$ modes, respectively. The higher p_T requirement on the latter is due to the higher average momentum required of the $\Xi_b(6227)^0$ baryon in order for all of its decay products to be within the LHCb detector acceptance. These selections provide an expected signal efficiency of about 55% and reduce the background by an order of magnitude.

C. $\Xi_b(6227)^-$ selection

The $\Xi_b(6227)^-$ candidates are formed by combining Λ_b^0 candidates in the mass interval 5560–5670 MeV and K^- candidates consistent with emerging from the same PV. A similar optimization to that discussed above is performed to determine the optimal p_T requirement on the K^- candidate. A loose PID requirement on the K^- candidate is applied in advance, which suppresses about 80% of the misidentified π^- background. Since the $\Xi_b(6227)^-$ state is established, the optimization uses $\mathrm{FOM} = N_S(p_T)/\sqrt{N_S(p_T) + N_B(p_T)}$, where $N_S(p_T) = \epsilon(p_T)N_{S0}$ is the expected signal yield based on an initial signal yield estimate, N_{S0}, and the efficiency, $\epsilon(p_T)$, obtained from simulation. The background yield, N_B, is obtained from wrong-sign $\Lambda_b^0 K^+$ combinations. The optimal requirement is $p_T > 1000$ MeV. The efficiency of this selection is about 40% and reduces the combinatorial background by a factor of ten.

With the $p_T > 1000$ MeV requirement applied, a more refined optimization is performed on the K^- PID requirement. The PID tuning for the 7 and 8 TeV data differs from that of the 13 TeV data [49], so different requirements are imposed. Using the same FOM as above, except with the PID variable used in place of the p_T, tighter PID requirements are imposed. The optimal PID requirement on the K^- candidate provides an efficiency of 80% (95%) while suppressing the background by a factor of 2 (1.6) for the Run 1 (Run 2) data samples. The same p_T and PID requirements are applied to the K^- candidate in both the $\Lambda_b^0 \to \Lambda_c^+\pi^-$ and $\Lambda_b^0 \to \Lambda_c^+\pi^-\pi^+\pi^-$ samples.

IV. FITS TO THE DATA

A. Fits to the Ξ_b^- and Λ_b^0 samples

An extended binned maximum-likelihood fit is performed to determine the Ξ_b^- and Λ_b^0 signal yields in the peaks shown in Figs. 1 and 2. The distributions are described by the sum of a signal function and three (two for Λ_b^0) background shapes to determine the signal yields. The signal shapes are described by the sum of two Crystal Ball functions [55] with a common value for the peak mass. For the Ξ_b^- modes, the signal shapes are fixed to the values obtained from simulation, except for the widths, which are allowed to vary freely in the fit. For the Λ_b^0 modes, the signal yields in data are significantly larger than in the simulated samples, and thus all signal shape parameters are freely varied in the fit. For both the Λ_b^0 and Ξ_b^- modes, there is background from $H_b \to H_c K^-(\pi^+\pi^-)$ decays, where the kaon is misidentified as a pion. This Cabibbo-suppressed (CS) contribution is small compared to the Cabibbo-favored (CF) $H_b \to H_c\pi^-\pi^+\pi^-$ decay. The CS to CF signal yield ratio is fixed to 1.8% based upon the PID efficiency of the K^- meson to pass the π^- PID requirement and the assumption that the CS/CF ratio of branching fractions is 7.3%, as is the case for $\mathcal{B}(\Lambda_b^0 \to \Lambda_c^+K^-)/\mathcal{B}(\Lambda_b^0 \to \Lambda_c^+\pi^-)$ [56]. For the Ξ_b^- modes, there is also a background contribution from $\Xi_b^- \to \Xi_c'^0\pi^-(\pi^+\pi^-)$ decays, where the photon from the decay $\Xi_c'^0 \to \Xi_c^0\gamma$ is not considered. The shapes of these background modes are taken from simulations and the yields are freely varied in the fit. Lastly, the combinatorial background shapes are parametrized as an exponential function with freely varying shape parameters and yields.

The results of the fit are superimposed in Figs. 1 and 2, and the fitted signal yields are shown in Tables I and II. In total, about 1.9 million Λ_b^0 and 16 000 Ξ_b^- signal decays are observed, with sizable contributions from final states containing three pions. The number of Λ_b^0 decays here is about four times larger than the sample used for the first measurement of the $\Xi_b(6227)^-$ mass and natural width [23].

B. Fit to the $\Xi_b(6227)^0 \to \Xi_b^-\pi^+$ sample

To search for the $\Xi_b(6227)^0$ state, the mass difference, $\delta M_\pi = M(\Xi_b^-\pi^+) - M(\Xi_b^-)$, is used, since the mass resolution on this difference is about eight times better than that of $M(\Xi_b^-\pi^+)$. Moreover, systematic uncertainties, particularly that due to the momentum scale calibration, are greatly reduced. The resulting mass difference spectra, δM_π, for both the right-sign and wrong-sign $(\Xi_b^-\pi^-)$ combinations are shown in Fig. 3. The top row shows

TABLE I. Signal yields of Ξ_b^- and $\Xi_b(6227)^0$ decays for the full data set after all selection requirements, and the corresponding Run 2 signal yields used for the measurement of $R(\Xi_b^-\pi^+)$ at 13 TeV.

	All data		$\sqrt{s}=13$ TeV
$\Xi_b^- \to$	$\Xi_c^0\pi^-$	$\Xi_c^0\pi^-\pi^+\pi^-$	$\Xi_c^0\pi^-$
$N(\Xi_b^-)$	$10\,800\pm400$	5100 ± 300	8300 ± 300
$N(\Xi_b(6227)^0\to\Xi_b^-\pi^+)$	176^{+33}_{-30}	86^{+19}_{-17}	150 ± 27

TABLE II. Signal yields of Λ_b^0 and $\Xi_b(6227)^-$ decays for the full data set after all selection requirements.

$\Lambda_b^0 \to$	$\Lambda_c^+\pi^-$	$\Lambda_c^+\pi^-\pi^+\pi^-$
$N(\Lambda_b^0)$ [10^3]	1214 ± 2	697 ± 1
$N(\Xi_b(6227)^-\to\Lambda_b^0K^-)$	1100 ± 108	1024 ± 106

the spectra using $\Xi_b^- \to \Xi_c^0\pi^-$ candidates and the bottom row shows the spectra using $\Xi_b^- \to \Xi_c^0\pi^-\pi^+\pi^-$ candidates. A clear signal is observed at the same invariant mass in both right-sign final states, while there are no significant structures in the wrong-sign spectra.

The $\Xi_b(6227)^0$ mass and natural width are obtained from a simultaneous unbinned maximum-likelihood fit to the four δM_π spectra. The signal shape is described by a P-wave relativistic Breit–Wigner function [57] with a Blatt–Weisskopf barrier factor [58] of 3 GeV^{-1}, convolved with a resolution function. The mass resolution is parametrized as the sum of two Gaussian functions with a common mean of zero and widths that are fixed to the values obtained from simulation. The weighted average mass resolution is about 2.0 MeV, which is negligible compared to the apparent width of the observed peak. The background shape is described by a smooth threshold function with shape parameters that are common between the right-sign and wrong-sign spectra, but independent for the $\Xi_c^0\pi^-$ and $\Xi_c^0\pi^-\pi^+\pi^-$ final states. The threshold function takes the form

$$\left(1+\tanh\left(\frac{\delta M_\pi-\delta M_0}{C}\right)\right)\times(\delta M_\pi-\delta M_0)^A. \qquad (3)$$

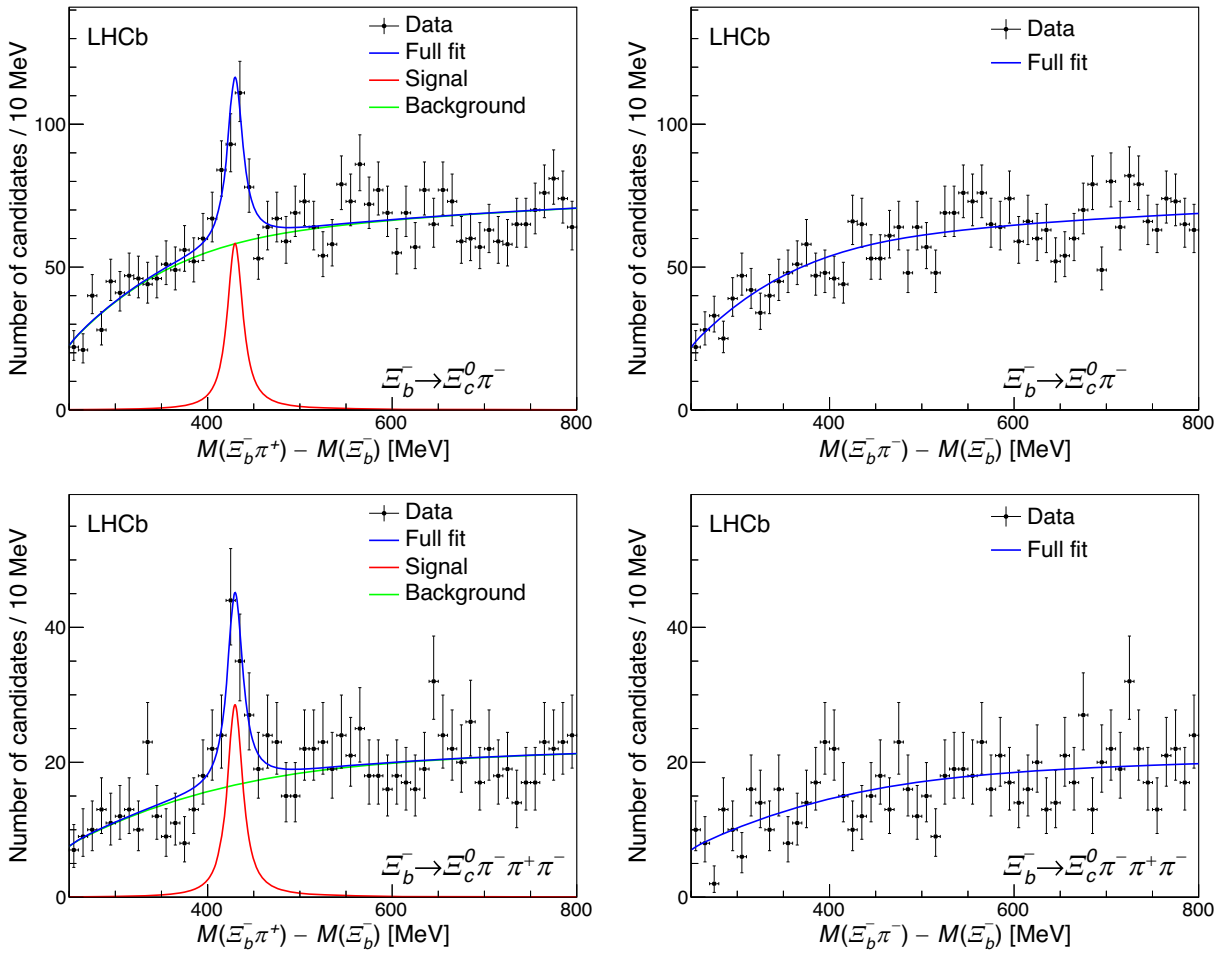

FIG. 3. Distribution of reconstructed $\delta M_\pi = M(\Xi_b^-\pi^+) - M(\Xi_b^-)$ in $\Xi_b(6227)^0 \to \Xi_b^-\pi^+$ candidate decays, with (top) $\Xi_b^- \to \Xi_c^0\pi^-$ decays, and (bottom) $\Xi_b^- \to \Xi_c^0\pi^-\pi^+\pi^-$ decays. The left column shows the right-sign candidates and the right column shows the wrong-sign candidates. The fit projections are overlaid.

The parameter δM_0 represents a threshold. Due to the low signal yield, the fit does not always converge when δM_0 is left to freely vary. Therefore, δM_0 is fixed to 240 MeV (10 MeV below the minimum of the fit range), and the value is varied as a source of systematic uncertainty. The parameters A and C are freely varied in the fit.

The projection of the fit is superimposed on the data in Fig. 3. Using the difference in log-likelihoods between the nominal fit and a fit where the signal yield is fixed to zero, a statistical significance of about 10σ is obtained. The $\Xi_b(6227)^0$ peak parameters are

$$\delta m_\pi^{\text{peak}} = 429.8^{+1.4}_{-1.5}\ \text{MeV},$$
$$m(\Xi_b(6227)^0) = 6227.1^{+1.4}_{-1.5}\ \text{MeV},$$
$$\Gamma(\Xi_b(6227)^0) = 18.6^{+5.0}_{-4.1}\ \text{MeV},$$

where the uncertainties are statistical only. The $\delta m_\pi^{\text{peak}}$ values obtained from independent fits to the two samples are consistent with one another, therefore justifying the combined fit. The $\Xi_b(6227)^0$ mass is obtained from $m(\Xi_b(6227)^0) = \delta m_\pi^{\text{peak}} + m(\Xi_b^-)$, where the value $m(\Xi_b^-) = 5797.33 \pm 0.24$ MeV obtained in this analysis is used, as discussed later. The fitted signal yields are shown in Table I.

C. Production ratio $R(\Xi_b^-\pi^+)$

The relative production rate is obtained from

$$R(\Xi_b^-\pi^+) = \frac{N(\Xi_b(6227)^0)}{N(\Xi_b^-)\epsilon_{\text{rel}}}, \tag{4}$$

where $N(\Xi_b(6227)^0)$ and $N(\Xi_b^-)$ are the signal yields and ϵ_{rel} is the relative efficiency between the $\Xi_b(6227)^0$ and Ξ_b^- selections. As the Ξ_b^- selection is common to both samples, the relative efficiency is predominantly due to the efficiency of reconstructing and selecting the π^+ meson.

About 80% of the signal is from the 13 TeV dataset, and therefore $R(\Xi_b^-\pi^+)$ is measured using only that subset of the data. In addition, the acceptance requirement $p_{\text{T}} < 30$ GeV and $2 < \eta < 5$ is applied to the reconstructed $\Xi_b(6227)^0$ candidates. To obtain $N(\Xi_b(6227)^0)$ and $N(\Xi_b^-)$, an alternative fit with only the 13 TeV data is performed, with the resulting $\Xi_b(6227)^0$ and Ξ_b^- signal yields shown in Table I. The Ξ_b^- signal yield is obtained by integrating the $\Xi_b^- \to \Xi_c^0\pi^-$, $\Xi_c^0 K^-$, and $\Xi_c'^0\pi^-$ signal shapes over the same mass interval ($5737 < M(\Xi_c^0\pi^-) < 5847$ MeV) that is used in the $\Xi_b(6227)^0$ selection. The $\Xi_c^0 K^-$, and $\Xi_c'^0\pi^-$ components are included in the Ξ_b^- yield because simulation shows that these misidentified Ξ_b^- decays also produce a narrow structure in the δM_π spectrum with approximately the same resolution as the $\Xi_c^0\pi^-$ signal.

The relative signal efficiency is obtained from the tuned simulation, from which the value $\epsilon_{\text{rel}} = (40.0 \pm 0.5)\%$ is obtained, where the uncertainty is due to the finite simulated sample sizes. Much of the efficiency loss is due to the $p_{\text{T}} > 700$ MeV requirement; with a less stringent requirement of $p_{\text{T}} > 200$ MeV, the relative efficiency is 75%. The efficiency includes a correction factor of 0.978 ± 0.021, which accounts for a slightly lower tracking efficiency in data than in simulation, as determined from an inclusive $J/\psi \to \mu^+\mu^-$ calibration sample [59], weighted to match the kinematics of the π^+ meson from the $\Xi_b(6227)^0$ decay.

With the signal yields in Table I and the above value of ϵ_{rel}, it is found that

$$R(\Xi_b^-\pi^+) = 0.045 \pm 0.008,$$

where the uncertainty is statistical only.

D. Fit to the $\Xi_b(6227)^- \to \Lambda_b^0 K^-$ sample

The spectra of mass differences, $\delta M_K = M(\Lambda_b^0 K^-) - M(\Lambda_b^0)$, are shown in Fig. 4 for the $\Lambda_b^0 \to \Lambda_c^+\pi^-$ and $\Lambda_b^0 \to \Lambda_c^+\pi^-\pi^+\pi^-$ modes. As with the $\Xi_b(6227)^0$ signal fit, an unbinned extended maximum-likelihood fit is performed. The wrong-sign spectra are not considered in the fit, since the δM_K background shape for the wrong-sign is visibly different from that of the right-sign. As for the $\Xi_b(6227)^0$ fit, the signal shape is described by a P-wave relativistic Breit–Wigner function with a Blatt–Weisskopf barrier factor convolved with a resolution function. The mass resolution is described by the sum of two Gaussian functions with a common mean of zero and widths that are fixed to the values obtained from simulation. The weighted-average width is about 1.4 MeV, which is small compared to the expected natural width of the signal peak. The background shape is given by the same functional form as Eq. (3), with the replacement $\delta M_\pi \to \delta M_K$ and δM_0 is fixed to the kaon mass [50]; the parameters A and C are freely varied in the fit.

The fit projections are superimposed to the data distributions in Fig. 4. The measured $\Xi_b(6227)^-$ peak parameters are

$$\delta m_K^{\text{peak}} = 608.3 \pm 0.8\ \text{MeV},$$
$$m(\Xi_b(6227)^-) = 6227.9 \pm 0.8\ \text{MeV},$$
$$\Gamma(\Xi_b(6227)^-) = 19.9 \pm 2.1\ \text{MeV},$$

where $m(\Lambda_b^0) = 5619.62 \pm 0.16 \pm 0.13$ MeV [60] is used to obtain $m(\Xi_b(6227)^-)$, with signal yields given in Table II. It is notable that the $\Xi_b(6227)^- \to (\Lambda_b^0 \to \Lambda_c^+\pi^-\pi^+\pi^-)K^-$ signal yield is about 90% of that of the $\Xi_b(6227)^- \to (\Lambda_b^0 \to \Lambda_c^+\pi^-)K^-$, even though the initial Λ_b^0 sample size is only about 57% as large. This enhancement is expected since the higher multiplicity final state must generally have larger p_{T} in order for all of its decay products to be reconstructed in the LHCb detector. Since the p_{T} of the $\Xi_b(6227)^-$ baryon is imparted to its decay

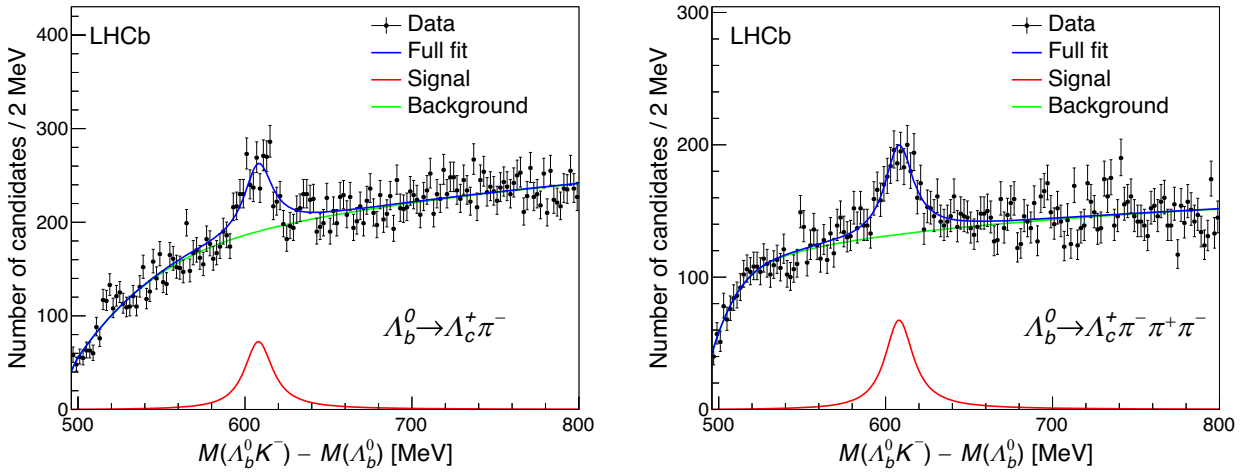

FIG. 4. Distribution of reconstructed $\delta M_K = M(\Lambda_b^0 K^-) - M(\Lambda_b^0)$ in $\Xi_b(6227)^- \to \Lambda_b^0 K^-$ candidate decays, with (left) $\Lambda_b^0 \to \Lambda_c^+ \pi^-$ and (right) $\Lambda_b^0 \to \Lambda_c^+ \pi^- \pi^+ \pi^-$ candidates. The fit projections are overlaid.

products, the reconstruction efficiency for the K^- meson is larger for the $\Xi_b(6227)^- \to (\Lambda_b^0 \to \Lambda_c^+ \pi^- \pi^+ \pi^-) K^-$ mode than the $\Xi_b(6227)^- \to (\Lambda_b^0 \to \Lambda_c^+ \pi^-) K^-$ mode.

E. Ξ_b^- mass measurement

The large Ξ_b^- and Λ_b^0 samples allow for a significant improvement in the uncertainty on the Ξ_b^- mass. Only the $H_b \to H_c \pi^-$ decays are used for this measurement. The lowest total uncertainty is achieved by measuring the mass difference, $m_{\rm diff} = m_{\rm fit}(\Xi_b^-) - m_{\rm fit}(\Lambda_b^0)$, where $m_{\rm fit}(\Xi_b^-)$ and $m_{\rm fit}(\Lambda_b^0)$ are the peak mass values from fits to the invariant-mass spectra. In $m_{\rm diff}$, the largest systematic uncertainty, the momentum scale calibration, is greatly reduced. The Ξ_b^- mass is then obtained from $m(\Xi_b^-) = m_{\rm diff} + m(\Lambda_b^0)$.

All of the previously discussed selection requirements are applied to the samples. Additionally, to render the Cabibbo-suppressed $H_b \to H_c K^-$ contribution negligible, a tighter PID requirement is applied to the pion coming directly from the H_b decay. This is done to avoid the systematic uncertainty associated with the shape and yield of a $H_b \to H_c K^-$ contribution in the mass fit. The efficiency of this additional selection is 89% for both the Λ_b^0 and Ξ_b^- signal decays.

The binned likelihood fits described previously are applied to the subset of data for this measurement, with the $H_b \to H_c K^-$ background shape removed. Separate fits are performed on the Run 1 (7 and 8 TeV), Run 2 (13 TeV) and the full data set. The invariant-mass spectra for Ξ_b^- and Λ_b^0 candidates and the fits to the full data sample are shown in Fig. 5, along with the full fit and the individual fit components. The numerical results of the mass fits for each running period and the combined data set are given in Table III. The different values of $m_{\rm fit}(\Lambda_b^0)$ for Run 1 and Run 2 are a result of the momentum scale uncertainty, which is greatly reduced in $m_{\rm diff}$. The values of $m_{\rm diff}$ are statistically compatible between the two running periods.

The Ξ_b^- mass is found to be

$$m(\Xi_b^-) = 5797.33 \pm 0.24 \text{ MeV},$$

where the uncertainty is statistical only.

TABLE III. The fitted signal yields and masses of the Ξ_b^- and Λ_b^0 peaks and the mass differences, $m_{\rm diff} \equiv m_{\rm fit}(\Xi_b^-) - m_{\rm fit}(\Lambda_b^0)$, for each center-of-mass energy and for the full data sample. For the last row, the known Λ_b^0 mass [60] is used. Uncertainties are statistical only.

	Run 1 (7 and 8 TeV)	Run 2 (13 TeV)	All data
$N(\Xi_b^-)$ [10^3]	1.9 ± 0.1	7.7 ± 0.2	9.6 ± 0.3
$N(\Lambda_b^0)$ [10^3]	226.7 ± 0.7	850.6 ± 1.2	1077.2 ± 1.3
$m_{\rm fit}(\Xi_b^-)$ [MeV]	5796.12 ± 0.57	5796.49 ± 0.26	5796.41 ± 0.24
$m_{\rm fit}(\Lambda_b^0)$ [MeV]	5618.10 ± 0.06	5618.85 ± 0.03	5618.70 ± 0.03
$m_{\rm diff}$ [MeV]	178.02 ± 0.57	177.64 ± 0.26	177.71 ± 0.24
$m(\Xi_b^-)$ [MeV]	5797.64 ± 0.57	5797.26 ± 0.26	5797.33 ± 0.24

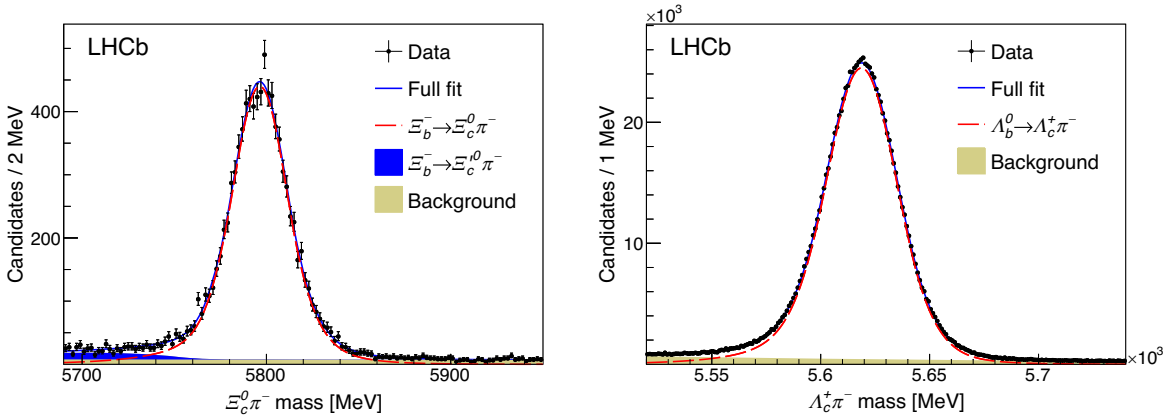

FIG. 5. Distribution of (left) $\Xi_c^0\pi^-$ and (right) $\Lambda_c^+\pi^-$ invariant mass for the combined Run 1 and Run 2 data sets, with extra PID selection requirements with respect to the samples shown in Figs. 1 and 2. The fit projections are overlaid.

V. SYSTEMATIC UNCERTAINTIES

Several sources of systematic uncertainty affect the measurements reported in this paper, and are summarized in Table IV.

A. $\Xi_b(6227)^0$ mass and natural width

To estimate the systematic effect of the background shape, three variations on the nominal fit are considered, including removing the wrong-sign data from the fit, varying the upper range of the mass fit by ± 100 MeV, and varying the δM_0 parameter in the background shape, which was fixed in the nominal fit, by ± 10 MeV. The maximum values among these variations, 0.1 MeV for $\delta m_\pi^{\text{peak}}$ and 1.4 MeV for $\Gamma(\Xi_b(6227)^0)$, are assigned as systematic uncertainty due to the background shape.

For the signal model, several alternative fits are investigated. Varying the barrier radius between 1 GeV^{-1} and 5 GeV^{-1}, and changing the relativistic Breit–Wigner function to model either an S- or D-wave decay, do not change the peak parameters significantly. The peak parameters are found to depend slightly on the assumed mass resolution. Varying the mass resolution by $\pm 10\%$ leads to a change in the peak mass and width of 0.1 MeV. A 0.1 MeV uncertainty is assigned to $\delta m_\pi^{\text{peak}}$ and the $\Xi_b(6227)^0$ width from the signal model.

The momentum scale calibration uncertainty, known to a precision of $\pm 0.03\%$ [61], largely cancels in the mass difference. To investigate the effect on $\delta m_\pi^{\text{peak}}$, the simulation is evaluated with the momentum scale shifted up and then down by this amount, leading to an uncertainty of 0.2 MeV. The energy loss uncertainty is estimated to be less than 0.1 MeV based upon the studies presented in Ref. [62]. A 0.1 MeV uncertainty is assigned.

In computing the uncertainty on $m(\Xi_b(6227)^0)$, the momentum scale and energy loss are taken to be 100%

TABLE IV. Summary of systematic uncertainties on quantities related to the $\Xi_b(6227)^0$ ($\delta m_\pi^{\text{peak}}$, $\Gamma(\Xi_b(6227)^0)$, $R(\Xi_b^-\pi^+)$), the $\Xi_b(6227)^-$ (δm_K^{peak}, $\Gamma(\Xi_b(6227)^-)$, and the Ξ_b^- mass (m_{diff}) measurements. The statistical uncertainties are also reported for comparison.

	$\Xi_b(6227)^0$			$\Xi_b(6227)^-$		Ξ_b^-
Source	$\delta m_\pi^{\text{peak}}$ [MeV]	Γ [MeV]	$R(\Xi_b^-\pi^+)$ [%]	δm_K^{peak} [MeV]	Γ [MeV]	m_{diff} [MeV]
$\Xi_b(6227)^0$ back. shape	0.1	1.4	5.6	-	-	-
$\Xi_b(6227)^0$ signal shape	0.1	0.1	0.7	-	-	-
$\Xi_b(6227)^-$ back. shape	-	-	-	0.4	1.5	-
$\Xi_b(6227)^-$ signal shape	-	-	-	0.0	0.1	-
Ξ_b^-, Λ_b^0 back. shape	-	-	1.5	-	-	0.08
Ξ_b^-, Λ_b^0 signal shape	-	-	2.0	-	-	0.10
Momentum scale	0.2	0.0	-	0.1	0.0	0.08
Energy loss	0.1	0.0	-	0.1	0.0	0.06
Production spectra	-	-	8.0	-	-	-
π^+ tracking efficiency	-	-	2.1	-	-	-
Simulated sample size	-	-	1.2	-	-	-
Total systematic	0.3	1.4	10.4	0.4	1.5	0.16
Statistical	$^{+1.4}_{-1.5}$	$^{+5.0}_{-4.1}$	18	0.8	2.1	0.24

correlated between $\delta m_\pi^{\rm peak}$ and $m(\Xi_b^-)$. The total systematic uncertainty is 0.3 MeV for $\delta m_\pi^{\rm peak}$, and 0.5 MeV and 1.4 MeV for the $\Xi_b(6227)^0$ mass and width, respectively.

B. $\Xi_b(6227)^-$ mass and natural width

Several variations to the nominal fit are performed to assess the background shape uncertainty. The variations include changing both the lower (by +20 MeV) and upper mass limits (by ±50 MeV) in the fit. The largest changes in the peak parameters, 0.4 MeV in $\delta m_K^{\rm peak}$ and 1.4 MeV in $\Gamma(\Xi_b(6227)^-)$, are assigned as systematic uncertainties. There is a small excess of events in the $\delta m_K^{\rm peak}$ spectrum in the data near 520 MeV. In an alternative fit, a second peak is included in the fit model for both mass spectra. The second peak is found to be statistically insignificant, however, its inclusion changes the $\Xi_b(6227)^-$ mass by 0.1 MeV and its width by 0.8 MeV. These values are added in quadrature with the values found from varying the fit range to arrive at a background systematic uncertainty of 0.4 MeV and 1.5 MeV on $\delta m_K^{\rm peak}$ and $\Gamma(\Xi_b(6227)^-)$, respectively.

For the signal model uncertainty, a similar set of variations is carried out as for the $\Xi_b(6227)^0$ case, and only the width shows any sensitivity to the ±10% variation in the mass resolution. The change of 0.1 MeV is assigned as an uncertainty on the $\Xi_b(6227)^-$ width.

The momentum and energy scale uncertainties each lead to a 0.1 MeV uncertainty on $\delta m_K^{\rm peak}$. In combining $\delta m_K^{\rm peak} = 608.3 \pm 0.8 \pm 0.4$ MeV with $m(\Lambda_b^0)$ [60] to obtain $m(\Xi_b(6227)^-)$, the momentum scale and energy loss portion of the systematic uncertainties are taken to be 100% correlated. The resulting systematic uncertainty on $m(\Xi_b(6227)^-)$ is 0.5 MeV.

C. Production ratio $R(\Xi_b^-\pi^+)$

In the measurement of $R(\Xi_b^-\pi^+)$, the sources of uncertainty include the signal and background shapes in the Ξ_b^- and $\Xi_b(6227)^0$ mass fits, and the relative efficiency estimate. For the Ξ_b^- mass fit, the signal yield is evaluated with an alternative signal model comprised of the sum of two Gaussian functions, where the means need not be the same and the widths are allowed to vary in the fit. The yield in this alternative fit changes by 2%, which is taken as a systematic error. The uncertainty due to the background shape is studied by changing to a Chebyshev polynomial, which leads to a 1.4% change in the yield. The upper end of the mass fit is reduced from 5950 MeV to 5900 MeV, and the 0.4% change in signal yield is assigned as systematic uncertainty. These two contributions are added in quadrature, resulting in an uncertainty of 1.5% due to the Ξ_b^- background shape.

Variations in the $\Xi_b(6227)^0$ background shape are also considered for the uncertainty on $R(\Xi_b^-\pi^+)$. The same set of variations that were performed for the $\Xi_b(6227)^0$ mass and width are considered. Adding the changes in yield in quadrature leads to a 5.6% uncertainty due to the $\Xi_b(6227)^0$ background shape. Several variations in the signal model are considered, and the only non-negligible change in signal yield occurs when a nonrelativistic Breit–Wigner function is used in place of the relativistic Breit–Wigner shape. The 0.7% change in the signal yield is assigned as an uncertainty to the $\Xi_b(6227)^0$ yield.

The relative efficiency depends on the extent to which the simulation properly models the $(p_{\rm T}, \eta)$ spectrum of Ξ_b^- and the $\Xi_b(6227)^0$ production spectra. The large Ξ_b^- sample allows for a precise tuning of the κ parameters, so that the $p_{\rm T}$ and η spectrum in simulation is well matched to that of the data. Due to the low signal yields in the $\Xi_b(6227)^0$ sample, it is estimated that the κ parameters have an uncertainty of ±0.005 units. A larger shift than 0.005 units leaves the simulation in clear disagreement with the background-subtracted data. Varying the κ_T parameter by this amount leads to an 8% change in $\epsilon_{\rm rel}$. This change is due almost entirely to the $p_{\rm T} > 700$ MeV requirement on the π^+ meson in the $\Xi_b(6227)^0$ decay. A ± 0.005 unit variation in κ_z is also investigated, but leads to a negligible change in the relative efficiency. The π^+ tracking efficiency correction has an uncertainty of 2.1%, which includes a 1.5% contribution from the calibration using $J/\psi \to \mu^+\mu^-$ decays and 1.4% due to the difference in material interactions between muons and pions [59]. The finite simulated sample sizes lead to an additional systematic uncertainty of 1.2%.

D. Ξ_b^- mass

The systematic uncertainty in $m_{\rm diff}$ is studied by performing alternative fits to the data, and assigning the change in $m_{\rm diff}$ with respect to the nominal value as a systematic uncertainty. The background shape uncertainty is estimated by using a Chebychev polynomial instead of the exponential background shape (0.05 MeV), reducing the upper limit of the fit range by 50 MeV (0.06 MeV), and fitting with a finer binning (0.02 MeV). The total background shape uncertainty is taken as the quadrature sum, which is 0.08 MeV. The signal shape uncertainty is assigned by changing the way the tail parameters are treated in the signal function. For the Ξ_b^- mass fit, they are changed from fixed values to floating values, and for the Λ_b^0, they are changed from floating values to fixed values based on the simulation. These variations lead to a change in $m_{\rm diff}$ of 0.10 MeV, which is assigned as the signal shape uncertainty. The momentum scale and energy loss uncertainties are unchanged from the previous result [63], and are 0.08 MeV and 0.06 MeV, respectively. Adding these uncertainties in quadrature, the total uncertainty on $m_{\rm diff}$ is 0.16 MeV.

In combining $m_{\rm diff} = 177.71 \pm 0.24 \pm 0.16$ MeV with $m(\Lambda_b^0)$ [60] to obtain $m(\Xi_b^-)$, the momentum scale and energy loss portion of the systematic uncertainties are taken to be 100% correlated. The remainder of the uncertainties

are taken to be uncorrelated. The resulting systematic uncertainty on $m(\Xi_b^-)$ is 0.29 MeV.

VI. SUMMARY

Using pp collision data at $\sqrt{s} = 7$, 8 and 13 TeV, corresponding to an integrated luminosity of 8.5 fb^{-1}, a new Ξ_b^0 baryon, referred to as $\Xi_b(6227)^0$, is reported with a statistical significance of 10σ. The mass difference, mass and natural width of the peak are measured to be

$$\begin{aligned}\delta m_\pi^{\text{peak}} &= 429.8^{+1.4}_{-1.5} \pm 0.3 \text{ MeV},\\ m(\Xi_b(6227)^0) &= 6227.1^{+1.4}_{-1.5} \pm 0.5 \text{ MeV},\\ \Gamma(\Xi_b(6227)^0) &= 18.6^{+5.0}_{-4.1} \pm 1.4 \text{ MeV},\end{aligned}$$

where the first uncertainty is statistical and the second is experimental systematic.

The relative production rate of the $\Xi_b(6227)^0$ state at $\sqrt{s} = 13$TeV is measured through its decay to $\Xi_b^-\pi^+$ to be

$$\begin{aligned}R(\Xi_b^-\pi^+) &\equiv \frac{f_{\Xi_b(6227)^0}}{f_{\Xi_b^-}}\mathcal{B}(\Xi_b(6227)^0 \to \Xi_b^-\pi^+)\\ &= 0.045 \pm 0.008 \pm 0.004.\end{aligned}$$

This is consistent with the values of $R(\Xi_b^0\pi^-)$ found in Ref. [23] for the $\Xi_b(6227)^-$ state. The value of $R(\Xi_b^-\pi^+)$ can also be compared to the corresponding value found for the lower-mass $\Xi_b(5945)^0$ state of $0.28 \pm 0.03 \pm 0.01$ [7]. Additional unobserved decay modes, such as $\Xi_b(5945)^0 \to \Xi_b^0\pi^0$ and $\Xi_b(6227)^0 \to (\Xi_b^0\pi^0, \Lambda_b^0\bar{K}^0)$, would clearly contribute to the total production rate of these excited states, but are yet to be observed.

From a sample of $\Xi_b(6227)^- \to \Lambda_b^0 K^-$ signal decays that is approximately four times larger than that which was used in the first observation of the $\Xi_b(6227)^-$ baryon [23], an updated measurement of the $\Xi_b(6227)^-$ mass and natural width is presented. The values obtained are

$$\begin{aligned}\delta m_K^{\text{peak}} &= 608.3 \pm 0.8 \pm 0.4 \text{ MeV},\\ m(\Xi_b(6227)^-) &= 6227.9 \pm 0.8 \pm 0.5 \text{ MeV},\\ \Gamma(\Xi_b(6227)^-) &= 19.9 \pm 2.1 \pm 1.5 \text{ MeV},\end{aligned}$$

which supersede the results in Ref. [23]. The measured masses of the $\Xi_b(6227)^0$ and $\Xi_b(6227)^-$ states are consistent with them being isospin partners.

Lastly, from a sample of about 10 000 $\Xi_b^- \to \Xi_c^0\pi^-$ and 1 million $\Lambda_b^0 \to \Lambda_c^+\pi^-$ signal decays, the mass difference between the two b baryons and the Ξ_b^- mass are measured to be

$$\begin{aligned}m_{\text{diff}} &= 177.71 \pm 0.24 \pm 0.16 \text{ MeV},\\ m(\Xi_b^-) &= 5797.33 \pm 0.24 \pm 0.29 \text{ MeV}.\end{aligned}$$

The result obtained here represents the single most precise determination of the Ξ_b^- mass. It is consistent with previous measurements and is about a factor of 1.6 times more precise than the current world average [50], and it supersedes the measurement reported in Ref. [63].

With the current data sample, it cannot be excluded that there are two or more narrower, closely spaced states contained within the peaks referred to as $\Xi_b(6227)^-$ and $\Xi_b(6227)^0$. With larger data samples in the future, it should be possible to probe whether these peaks are comprised of narrower states.

ACKNOWLEDGMENTS

We express our gratitude to our colleagues in the CERN accelerator departments for the excellent performance of the LHC. We thank the technical and administrative staff at the LHCb institutes. We acknowledge support from CERN and from the national agencies: CAPES, CNPq, FAPERJ and FINEP (Brazil); MOST and NSFC (China); CNRS/IN2P3 (France); BMBF, DFG and MPG (Germany); INFN (Italy); NWO (Netherlands); MNiSW and NCN (Poland); MEN/IFA (Romania); MSHE (Russia); MICINN (Spain); SNSF and SER (Switzerland); NASU (Ukraine); STFC (United Kingdom); DOE NP and NSF (USA). We acknowledge the computing resources that are provided by CERN, IN2P3 (France), KIT and DESY (Germany), INFN (Italy), SURF (Netherlands), PIC (Spain), GridPP (United Kingdom), RRCKI and Yandex LLC (Russia), CSCS (Switzerland), IFIN-HH (Romania), CBPF (Brazil), PL-GRID (Poland) and OSC (USA). We are indebted to the communities behind the multiple open-source software packages on which we depend. Individual groups or members have received support from AvH Foundation (Germany); EPLANET, Marie Skłodowska-Curie Actions and ERC (European Union); A*MIDEX, ANR, Labex P2IO and OCEVU, and Région Auvergne-Rhône-Alpes (France); Key Research Program of Frontier Sciences of CAS, CAS PIFI, Thousand Talents Program, and Sci. & Tech. Program of Guangzhou (China); RFBR, RSF and Yandex LLC (Russia); GVA, XuntaGal and GENCAT (Spain); the Royal Society and the Leverhulme Trust (United Kingdom).

[1] M. Gell-Mann, A schematic model of baryons and mesons, Phys. Lett. **8**, 214 (1964).

[2] G. Zweig, An SU_3 model for strong interaction symmetry and its breaking; Version 1 Report No. CERN-TH-401, CERN, Geneva, 1964.

[3] E. Klempt and J.-M. Richard, Baryon spectroscopy, Rev. Mod. Phys. **82**, 1095 (2010).

[4] D. Ebert, T. Feldmann, C. Kettner, and H. Reinhardt, A diquark model for baryons containing one heavy quark, Z. Phys. C **71**, 329 (1996).

[5] R. Aaij *et al.* (LHCb Collaboration), Observation of Two New Ξ_b^- Baryon Resonances, Phys. Rev. Lett. **114**, 062004 (2015).

[6] S. Chatrchyan *et al.* (CMS Collaboration), Observation of a New Ξ_b Baryon, Phys. Rev. Lett. **108**, 252002 (2012).

[7] R. Aaij *et al.* (LHCb Collaboration), Measurement of the properties of the Ξ_b^{*0} baryon, J. High Energy Phys. 05 (2016) 161.

[8] D. Ebert, R. N. Faustov, and V. O. Galkin, Spectroscopy and Regge trajectories of heavy baryons in the relativistic quark-diquark picture, Phys. Rev. D **84**, 014025 (2011).

[9] D. Ebert, R. N. Faustov, and V. O. Galkin, Masses of excited heavy baryons in the relativistic quark-diquark picture, Phys. Lett. B **659**, 612 (2008).

[10] W. Roberts and M. Pervin, Heavy baryons in a quark model, Int. J. Mod. Phys. A **23**, 2817 (2008).

[11] H. Garcilazo, J. Vijande, and A. Valcarce, Faddeev study of heavy-baryon spectroscopy, J. Phys. G **34**, 961 (2007).

[12] B. Chen, K.-W. Wei, and A. Zhang, Investigation of Λ_Q and Ξ_Q baryons in the heavy quark-light diquark picture, Eur. Phys. J. A **51**, 82 (2015).

[13] Q. Mao, H.-X. Chen, W. Chen, A. Hosaka, X. Liu, and S.-L. Zhu, QCD sum rule calculation for P-wave bottom baryons, Phys. Rev. D **92**, 114007 (2015).

[14] C. Garcia-Recio, J. Nieves, O. Romanets, L. L. Salcedo, and L. Tolos, Odd parity bottom-flavored baryon resonances, Phys. Rev. D **87**, 034032 (2013).

[15] M. Karliner, B. Keren-Zur, H. J. Lipkin, and J. L. Rosner, The quark model and b baryons, Ann. Phys. (Amsterdam) **324**, 2 (2009).

[16] Z.-G. Wang, Analysis of the $1/2^-$ and $3/2^-$ heavy and doubly heavy baryon states with QCD sum rules, Eur. Phys. J. A **47**, 81 (2011).

[17] A. Valcarce, H. Garcilazo, and J. Vijande, Towards an understanding of heavy baryon spectroscopy, Eur. Phys. J. A **37**, 217 (2008).

[18] J. Vijande, A. Valcarce, T. F. Carames, and H. Garcilazo, Heavy hadron spectroscopy: a quark model perspective, Int. J. Mod. Phys. E **22**, 1330011 (2013).

[19] K.-L. Wang, Y.-X. Yao, X.-H. Zhong, and Q. Zhao, Strong and radiative decays of the low-lying S- and P-wave singly heavy baryons, Phys. Rev. D **96**, 116016 (2017).

[20] Z.-Y. Wang, J.-J. Qi, X.-H. Guo, and K.-W. Wei, Spectra of charmed and bottom baryons with hyperfine interaction, Chin. Phys. C **41**, 093103 (2017).

[21] H.-X. Chen, Q. Mao, A. Hosaka, X. Liu, and S.-L. Zhu, D-wave charmed and bottomed baryons from QCD sum rules, Phys. Rev. D **94**, 114016 (2016).

[22] K. Thakkar, Z. Shah, A. K. Rai, and P. C. Vinodkumar, Excited state mass spectra and Regge trajectories of bottom baryons, Nucl. Phys. **A965**, 57 (2017).

[23] R. Aaij *et al.* (LHCb Collaboration), Observation of a New Ξ_b^- Resonance, Phys. Rev. Lett. **121**, 072002 (2018).

[24] K.-L. Wang, Q.-F. L, and X.-H. Zhong, Interpretation of the newly observed $\Sigma_b(6097)^{\pm}$ and $\Xi_b(6227)^-$ states as the P-wave bottom baryons, Phys. Rev. D **99**, 014011 (2019).

[25] B. Chen, K.-W. Wei, X. Liu, and A. Zhang, Role of newly discovered $\Xi_b(6227)^-$ for constructing excited bottom baryon family, Phys. Rev. D **98**, 031502 (2018).

[26] B. Chen and X. Liu, Assigning the newly reported $\Sigma_b(6097)$ as a P-wave excited state and predicting its partners, Phys. Rev. D **98**, 074032 (2018).

[27] T. M. Aliev, K. Azizi, Y. Sarac, and H. Sundu, Structure of the $\Xi_b(6227)^-$ resonance, Phys. Rev. D **98**, 094014 (2018).

[28] E.-L. Cui, H.-M. Yang, H.-X. Chen, and A. Hosaka, Identifying the $\Xi_b(6227)$ and $\Sigma_b(6097)$ as P-wave bottom baryons of $J^P = 3/2^-$, Phys. Rev. D **99**, 094021 (2019).

[29] H.-M. Yang, H.-X. Chen, E.-L. Cui, A. Hosaka, and Q. Mao, Decay properties of P-wave bottom baryons within light-cone sum rules, Eur. Phys. J. C **80**, 80 (2020).

[30] H.-M. Yang and H.-X. Chen, P-wave bottom baryons of the $SU(3)$ flavor $\mathbf{6}_F$, Phys. Rev. D **101**, 114013 (2020).

[31] R. N. Faustov and V. O. Galkin, Heavy baryon spectroscopy in the relativistic quark model, Particles **3**, 234 (2020).

[32] R. N. Faustov and V. O. Galkin, Heavy baryon spectroscopy, EPJ Web Conf. **204**, 08001 (2019).

[33] D. Jia, W.-N. Liu, and A. Hosaka, Regge behaviors in orbitally excited spectroscopy of charmed and bottom baryons, Phys. Rev. D **101**, 034016 (2020).

[34] Y. Kim, E. Hiyama, M. Oka, and K. Suzuki, Spectrum of singly heavy baryons from a chiral effective theory of diquarks, Phys. Rev. D **102**, 014004 (2020).

[35] H. Zhu and Y. Huang, Radiative decay of $\Xi_b(6227)$ in a hadronic molecule picture, Chin. Phys. C **44**, 083101 (2020).

[36] Q. X. Yu, R. Pavao, V. R. Debastiani, and E. Oset, Description of the Ξ_c and Ξ_b states as molecular states, Eur. Phys. J. C **79**, 167 (2019).

[37] J. Nieves, R. Pavao, and L. Tolos, Ξ_c and Ξ_b excited states within a $\mathrm{SU}(6)_{\mathrm{lsf}} \times$ HQSS model, Eur. Phys. J. C **80**, 22 (2020).

[38] Y. Huang, C.-J. Xiao, L.-S. Geng, and J. He, Strong decays of the $\Xi_b(6227)$ as a $\Sigma_b \bar{K}$ molecule, Phys. Rev. D **99**, 014008 (2019).

[39] A. A. Alves, Jr. *et al.* (LHCb Collaboration), The LHCb detector at the LHC, J. Instrum. **3**, S08005 (2008).

[40] R. Aaij *et al.* (LHCb Collaboration), LHCb detector performance, Int. J. Mod. Phys. A **30**, 1530022 (2015).

[41] T. Sjöstrand, S. Mrenna, and P. Skands, A brief introduction to PYTHIA 8.1, Comput. Phys. Commun. **178**, 852 (2008); T. Sjöstrand, S. Mrenna, and P. Skands, PYTHIA 6.4 physics and manual, J. High Energy Phys. 05 (2006) 026.

[42] I. Belyaev *et al.*, Handling of the generation of primary events in Gauss, the LHCb simulation framework, J. Phys. Conf. Ser. **331**, 032047 (2011).

[43] D. J. Lange, The EvtGen particle decay simulation package, Nucl. Instrum. Methods Phys. Res., Sect. A **462**, 152 (2001).

[44] P. Golonka and Z. Was, PHOTOS Monte Carlo: A precision tool for QED corrections in Z and W decays, Eur. Phys. J. C **45**, 97 (2006).

[45] J. Allison *et al.* (Geant4 Collaboration), GEANT4 developments and applications, IEEE Trans. Nucl. Sci. **53**, 270 (2006); S. Agostinelli *et al.* (Geant4 Collaboration), GEANT4: A simulation toolkit, Nucl. Instrum. Methods Phys. Res., Sect. A **506**, 250 (2003).

[46] M. Clemencic, G. Corti, S. Easo, C. R. Jones, S. Miglioranzi, M. Pappagallo, and P. Robbe, The LHCb simulation application, Gauss: Design, evolution and experience, J. Phys. Conf. Ser. **331**, 032023 (2011).

[47] M. Pivk and F. R. Le Diberder, sPlot: A statistical tool to unfold data distributions, Nucl. Instrum. Methods Phys. Res., Sect. A **555**, 356 (2005).

[48] M. Adinolfi *et al.*, Performance of the LHCb RICH detector at the LHC, Eur. Phys. J. C **73**, 2431 (2013).

[49] R. Aaij *et al.*, Selection and processing of calibration samples to measure the particle identification performance of the LHCb experiment in Run 2, Eur. Phys. J. Tech. Instr. **6**, 1 (2018).

[50] P. A. Zyla *et al.* (Particle Data Group), Review of particle physics, Prog. Theor. Exp. Phys. **2020**, 083C01 (2020).

[51] B. P. Roe, H.-J. Yang, J. Zhu, Y. Liu, I. Stancu, and G. McGregor, Boosted decision trees as an alternative to artificial neural networks for particle identification, Nucl. Instrum. Methods Phys. Res., Sect. A **543**, 577 (2005).

[52] Y. Freund and R. E. Schapire, A decision-theoretic generalization of on-line learning and an application to boosting, J. Comput. Syst. Sci. **55**, 119 (1997).

[53] H. Voss, A. Hoecker, J. Stelzer, and F. Tegenfeldt, TMVA—Toolkit for multivariate data analysis with ROOT, Proc. Sci., ACAT2007 (**2007**) 040.

[54] G. Punzi, Sensitivity of searches for new signals and its optimization, eConf **C030908**, MODT002 (2003).

[55] T. Skwarnicki, A study of the radiative cascade transitions between the Upsilon-prime and Upsilon resonances, PhD thesis, Institute of Nuclear Physics, Krakow, 1986 [Report No. DESY-F31-86-02].

[56] R. Aaij *et al.* (LHCb Collaboration), Study of beauty baryon decays to $D^0\mathrm{p}h^-$ and $\Lambda_c^+ h^-$ final states, Phys. Rev. D **89**, 032001 (2014).

[57] J. D. Jackson, Remarks on the phenomenological analysis of resonances, Nuovo Cimento **34**, 1644 (1964).

[58] J. M. Blatt and V. F. Weisskopf, Theoretical nuclear physics, *Dover Books on Physics* (Springer, New York, NY, 1979). This book has also been published by Dover in 1991.

[59] R. Aaij *et al.* (LHCb Collaboration), Measurement of the track reconstruction efficiency at LHCb, J. Instrum. **10**, P02007 (2015).

[60] R. Aaij *et al.* (LHCb Collaboration), Observation of the Decays $\Lambda_b^0 \to \chi_{c1} p K^-$ and $\Lambda_b^0 \to \chi_{c2} p K^-$, Phys. Rev. Lett. **119**, 062001 (2017).

[61] R. Aaij *et al.* (LHCb Collaboration), Precision measurement of D meson mass differences, J. High Energy Phys. 06 (2013) 065.

[62] R. Aaij *et al.* (LHCb Collaboration), Measurement of b -hadron masses, Phys. Lett. B **708**, 241 (2012).

[63] R. Aaij *et al.* (LHCb Collaboration), Precision Measurement of the Mass and Lifetime of the Ξ_b^- Baryon, Phys. Rev. Lett. **113**, 242002 (2014).

R. Aaij,[31] C. Abellán Beteta,[49] T. Ackernley,[59] B. Adeva,[45] M. Adinolfi,[53] H. Afsharnia,[9] C. A. Aidala,[84] S. Aiola,[25] Z. Ajaltouni,[9] S. Akar,[64] J. Albrecht,[14] F. Alessio,[47] M. Alexander,[58] A. Alfonso Albero,[44] Z. Aliouche,[61] G. Alkhazov,[37] P. Alvarez Cartelle,[47] S. Amato,[2] Y. Amhis,[11] L. An,[21] L. Anderlini,[21] A. Andreianov,[37] M. Andreotti,[20] F. Archilli,[16] A. Artamonov,[43] M. Artuso,[67] K. Arzymatov,[41] E. Aslanides,[10] M. Atzeni,[49] B. Audurier,[11] S. Bachmann,[16] M. Bachmayer,[48] J. J. Back,[55] S. Baker,[60] P. Baladron Rodriguez,[45] V. Balagura,[11] W. Baldini,[20] J. Baptista Leite,[1] R. J. Barlow,[61] S. Barsuk,[11] W. Barter,[60] M. Bartolini,[23,a] F. Baryshnikov,[80] J. M. Basels,[13] G. Bassi,[28] B. Batsukh,[67] A. Battig,[14] A. Bay,[48] M. Becker,[14] F. Bedeschi,[28] I. Bediaga,[1] A. Beiter,[67] V. Belavin,[41] S. Belin,[26] V. Bellee,[48] K. Belous,[43] I. Belov,[39] I. Belyaev,[38] G. Bencivenni,[22] E. Ben-Haim,[12] A. Berezhnoy,[39] R. Bernet,[49] D. Berninghoff,[16] H. C. Bernstein,[67] C. Bertella,[47] E. Bertholet,[12] A. Bertolin,[27] C. Betancourt,[49] F. Betti,[19,b] M. O. Bettler,[54] Ia. Bezshyiko,[49] S. Bhasin,[53] J. Bhom,[33] L. Bian,[72] M. S. Bieker,[14] S. Bifani,[52] P. Billoir,[12] M. Birch,[60] F. C. R. Bishop,[54] A. Bizzeti,[21,c] M. Bjørn,[62] M. P. Blago,[47] T. Blake,[55] F. Blanc,[48] S. Blusk,[67] D. Bobulska,[58] J. A. Boelhauve,[14] O. Boente Garcia,[45] T. Boettcher,[63] A. Boldyrev,[81] A. Bondar,[42] N. Bondar,[37] S. Borghi,[61] M. Borisyak,[41] M. Borsato,[16] J. T. Borsuk,[33] S. A. Bouchiba,[48] T. J. V. Bowcock,[59] A. Boyer,[47] C. Bozzi,[20] M. J. Bradley,[60] S. Braun,[65] A. Brea Rodriguez,[45] M. Brodski,[47] J. Brodzicka,[33] A. Brossa Gonzalo,[55] D. Brundu,[26] A. Buonaura,[49] C. Burr,[47] A. Bursche,[26] A. Butkevich,[40] J. S. Butter,[31] J. Buytaert,[47] W. Byczynski,[47] S. Cadeddu,[26] H. Cai,[72] R. Calabrese,[20,d] L. Calefice,[14,12] L. Calero Diaz,[22] S. Cali,[22] R. Calladine,[52] M. Calvi,[24,e] M. Calvo Gomez,[83] P. Camargo Magalhaes,[53] A. Camboni,[44] P. Campana,[22] D. H. Campora Perez,[47] A. F. Campoverde Quezada,[5] S. Capelli,[24,e] L. Capriotti,[19,b] A. Carbone,[19,b] G. Carboni,[29] R. Cardinale,[23,a] A. Cardini,[26] I. Carli,[6] P. Carniti,[24,e] K. Carvalho Akiba,[31] A. Casais Vidal,[45] G. Casse,[59] M. Cattaneo,[47] G. Cavallero,[47] S. Celani,[48] J. Cerasoli,[10] A. J. Chadwick,[59] M. G. Chapman,[53] M. Charles,[12] Ph. Charpentier,[47] G. Chatzikonstantinidis,[52] C. A. Chavez Barajas,[59] M. Chefdeville,[8] C. Chen,[3] S. Chen,[26] A. Chernov,[33] S.-G. Chitic,[47] V. Chobanova,[45] S. Cholak,[48]

M. Chrzaszcz,[33] A. Chubykin,[37] V. Chulikov,[37] P. Ciambrone,[22] M. F. Cicala,[55] X. Cid Vidal,[45] G. Ciezarek,[47] P. E. L. Clarke,[57] M. Clemencic,[47] H. V. Cliff,[54] J. Closier,[47] J. L. Cobbledick,[61] V. Coco,[47] J. A. B. Coelho,[11] J. Cogan,[10] E. Cogneras,[9] L. Cojocariu,[36] P. Collins,[47] T. Colombo,[47] L. Congedo,[18,f] A. Contu,[26] N. Cooke,[52] G. Coombs,[58] G. Corti,[47] C. M. Costa Sobral,[55] B. Couturier,[47] D. C. Craik,[63] J. Crkovská,[66] M. Cruz Torres,[1] R. Currie,[57] C. L. Da Silva,[66] E. Dall'Occo,[14] J. Dalseno,[45] C. D'Ambrosio,[47] A. Danilina,[38] P. d'Argent,[47] A. Davis,[61] O. De Aguiar Francisco,[61] K. De Bruyn,[77] S. De Capua,[61] M. De Cian,[48] J. M. De Miranda,[1] L. De Paula,[2] M. De Serio,[18,f] D. De Simone,[49] P. De Simone,[22] J. A. de Vries,[78] C. T. Dean,[66] W. Dean,[84] D. Decamp,[8] L. Del Buono,[12] B. Delaney,[54] H.-P. Dembinski,[14] A. Dendek,[34] V. Denysenko,[49] D. Derkach,[81] O. Deschamps,[9] F. Desse,[11] F. Dettori,[26,g] B. Dey,[72] P. Di Nezza,[22] S. Didenko,[80] L. Dieste Maronas,[45] H. Dijkstra,[47] V. Dobishuk,[51] A. M. Donohoe,[17] F. Dordei,[26] A. C. dos Reis,[1] L. Douglas,[58] A. Dovbnya,[50] A. G. Downes,[8] K. Dreimanis,[59] M. W. Dudek,[33] L. Dufour,[47] V. Duk,[76] P. Durante,[47] J. M. Durham,[66] D. Dutta,[61] M. Dziewiecki,[16] A. Dziurda,[33] A. Dzyuba,[37] S. Easo,[56] U. Egede,[68] V. Egorychev,[38] S. Eidelman,[42,h] S. Eisenhardt,[57] S. Ek-In,[48] L. Eklund,[58] S. Ely,[67] A. Ene,[36] E. Epple,[66] S. Escher,[13] J. Eschle,[49] S. Esen,[31] T. Evans,[47] A. Falabella,[19] J. Fan,[3] Y. Fan,[5] B. Fang,[72] N. Farley,[52] S. Farry,[59] D. Fazzini,[24,e] P. Fedin,[38] M. Féo,[47] P. Fernandez Declara,[47] A. Fernandez Prieto,[45] J. M. Fernandez-tenllado Arribas,[44] F. Ferrari,[19,b] L. Ferreira Lopes,[48] F. Ferreira Rodrigues,[2] S. Ferreres Sole,[31] M. Ferrillo,[49] M. Ferro-Luzzi,[47] S. Filippov,[40] R. A. Fini,[18] M. Fiorini,[20,d] M. Firlej,[34] K. M. Fischer,[62] C. Fitzpatrick,[61] T. Fiutowski,[34] F. Fleuret,[11,i] M. Fontana,[12] F. Fontanelli,[23,a] R. Forty,[47] V. Franco Lima,[59] M. Franco Sevilla,[65] M. Frank,[47] E. Franzoso,[20] G. Frau,[16] C. Frei,[47] D. A. Friday,[58] J. Fu,[25] Q. Fuehring,[14] W. Funk,[47] E. Gabriel,[31] T. Gaintseva,[41] A. Gallas Torreira,[45] D. Galli,[19,b] S. Gambetta,[57,47] Y. Gan,[3] M. Gandelman,[2] P. Gandini,[25] Y. Gao,[4] M. Garau,[26] L. M. Garcia Martin,[55] P. Garcia Moreno,[44] J. García Pardiñas,[49] B. Garcia Plana,[45] F. A. Garcia Rosales,[11] L. Garrido,[44] C. Gaspar,[47] R. E. Geertsema,[31] D. Gerick,[16] L. L. Gerken,[14] E. Gersabeck,[61] M. Gersabeck,[61] T. Gershon,[55] D. Gerstel,[10] Ph. Ghez,[8] V. Gibson,[54] M. Giovannetti,[22,j] A. Gioventù,[45] P. Gironella Gironell,[44] L. Giubega,[36] C. Giugliano,[20,47,d] K. Gizdov,[57] E. L. Gkougkousis,[47] V. V. Gligorov,[12] C. Göbel,[69] E. Golobardes,[83] D. Golubkov,[38] A. Golutvin,[60,80] A. Gomes,[1,k] S. Gomez Fernandez,[44] F. Goncalves Abrantes,[69] M. Goncerz,[33] G. Gong,[3] P. Gorbounov,[38] I. V. Gorelov,[39] C. Gotti,[24,e] E. Govorkova,[47] J. P. Grabowski,[16] R. Graciani Diaz,[44] T. Grammatico,[12] L. A. Granado Cardoso,[47] E. Graugés,[44] E. Graverini,[48] G. Graziani,[21] A. Grecu,[36] L. M. Greeven,[31] P. Griffith,[20] L. Grillo,[61] S. Gromov,[80] B. R. Gruberg Cazon,[62] C. Gu,[3] M. Guarise,[20] P. A. Günther,[16] E. Gushchin,[40] A. Guth,[13] Y. Guz,[43,47] T. Gys,[47] T. Hadavizadeh,[68] G. Haefeli,[48] C. Haen,[47] J. Haimberger,[47] S. C. Haines,[54] T. Halewood-leagas,[59] P. M. Hamilton,[65] Q. Han,[7] X. Han,[16] T. H. Hancock,[62] S. Hansmann-Menzemer,[16] N. Harnew,[62] T. Harrison,[59] C. Hasse,[47] M. Hatch,[47] J. He,[5] M. Hecker,[60] K. Heijhoff,[31] K. Heinicke,[14] A. M. Hennequin,[47] K. Hennessy,[59] L. Henry,[25,46] J. Heuel,[13] A. Hicheur,[2] D. Hill,[62] M. Hilton,[61] S. E. Hollitt,[14] J. Hu,[16] J. Hu,[71] W. Hu,[7] W. Huang,[5] X. Huang,[72] W. Hulsbergen,[31] R. J. Hunter,[55] M. Hushchyn,[81] D. Hutchcroft,[59] D. Hynds,[31] P. Ibis,[14] M. Idzik,[34] D. Ilin,[37] P. Ilten,[64] A. Inglessi,[37] A. Ishteev,[80] K. Ivshin,[37] R. Jacobsson,[47] S. Jakobsen,[47] E. Jans,[31] B. K. Jashal,[46] A. Jawahery,[65] V. Jevtic,[14] M. Jezabek,[33] F. Jiang,[3] M. John,[62] D. Johnson,[47] C. R. Jones,[54] T. P. Jones,[55] B. Jost,[47] N. Jurik,[47] S. Kandybei,[50] Y. Kang,[3] M. Karacson,[47] N. Kazeev,[81] F. Keizer,[54,47] M. Kenzie,[55] T. Ketel,[32] B. Khanji,[14] A. Kharisova,[82] S. Kholodenko,[43] K. E. Kim,[67] T. Kirn,[13] V. S. Kirsebom,[48] O. Kitouni,[63] S. Klaver,[31] K. Klimaszewski,[35] S. Koliiev,[51] A. Kondybayeva,[80] A. Konoplyannikov,[38] P. Kopciewicz,[34] R. Kopecna,[16] P. Koppenburg,[31] M. Korolev,[39] I. Kostiuk,[31,51] O. Kot,[51] S. Kotriakhova,[37,30] P. Kravchenko,[37] L. Kravchuk,[40] R. D. Krawczyk,[47] M. Kreps,[55] F. Kress,[60] S. Kretzschmar,[13] P. Krokovny,[42,h] W. Krupa,[34] W. Krzemien,[35] W. Kucewicz,[33,l] M. Kucharczyk,[33] V. Kudryavtsev,[42,h] H. S. Kuindersma,[31] G. J. Kunde,[66] T. Kvaratskheliya,[38] D. Lacarrere,[47] G. Lafferty,[61] A. Lai,[26] A. Lampis,[26] D. Lancierini,[49] J. J. Lane,[61] R. Lane,[53] G. Lanfranchi,[22] C. Langenbruch,[13] J. Langer,[14] O. Lantwin,[49,80] T. Latham,[55] F. Lazzari,[28,m] R. Le Gac,[10] S. H. Lee,[84] R. Lefèvre,[9] A. Leflat,[39] S. Legotin,[80] O. Leroy,[10] T. Lesiak,[33] B. Leverington,[16] H. Li,[71] L. Li,[62] P. Li,[16] X. Li,[66] Y. Li,[6] Y. Li,[6] Z. Li,[67] X. Liang,[67] T. Lin,[60] R. Lindner,[47] V. Lisovskyi,[14] R. Litvinov,[26] G. Liu,[71] H. Liu,[5] S. Liu,[6] X. Liu,[3] A. Loi,[26] J. Lomba Castro,[45] I. Longstaff,[58] J. H. Lopes,[2] G. Loustau,[49] G. H. Lovell,[54] Y. Lu,[6] D. Lucchesi,[27,n] S. Luchuk,[40] M. Lucio Martinez,[31] V. Lukashenko,[31] Y. Luo,[3] A. Lupato,[61] E. Luppi,[20,d] O. Lupton,[55] A. Lusiani,[28,o] X. Lyu,[5] L. Ma,[6] S. Maccolini,[19,b] F. Machefert,[11] F. Maciuc,[36] V. Macko,[48] P. Mackowiak,[14] S. Maddrell-Mander,[53] O. Madejczyk,[34] L. R. Madhan Mohan,[53] O. Maev,[37] A. Maevskiy,[81] D. Maisuzenko,[37] M. W. Majewski,[34] S. Malde,[62] B. Malecki,[47] A. Malinin,[79] T. Maltsev,[42,h] H. Malygina,[16] G. Manca,[26,g] G. Mancinelli,[10] R. Manera Escalero,[44] D. Manuzzi,[19,b] D. Marangotto,[25,p] J. Maratas,[9,q] J. F. Marchand,[8] U. Marconi,[19] S. Mariani,[21,47,r] C. Marin Benito,[11] M. Marinangeli,[48] P. Marino,[48] J. Marks,[16] P. J. Marshall,[59] G. Martellotti,[30] L. Martinazzoli,[47,e] M. Martinelli,[24,e] D. Martinez Santos,[45]

F. Martinez Vidal,[46] A. Massafferri,[1] M. Materok,[13] R. Matev,[47] A. Mathad,[49] Z. Mathe,[47] V. Matiunin,[38] C. Matteuzzi,[24] K. R. Mattioli,[84] A. Mauri,[31] E. Maurice,[11,i] J. Mauricio,[44] M. Mazurek,[35] M. McCann,[60] L. Mcconnell,[17] T. H. Mcgrath,[61] A. McNab,[61] R. McNulty,[17] J. V. Mead,[59] B. Meadows,[64] C. Meaux,[10] G. Meier,[14] N. Meinert,[75] D. Melnychuk,[35] S. Meloni,[24,e] M. Merk,[31,78] A. Merli,[25] L. Meyer Garcia,[2] M. Mikhasenko,[47] D. A. Milanes,[73] E. Millard,[55] M. Milovanovic,[47] M.-N. Minard,[8] L. Minzoni,[20,d] S. E. Mitchell,[57] B. Mitreska,[61] D. S. Mitzel,[47] A. Mödden,[14] R. A. Mohammed,[62] R. D. Moise,[60] T. Mombächer,[14] I. A. Monroy,[73] S. Monteil,[9] M. Morandin,[27] G. Morello,[22] M. J. Morello,[28,o] J. Moron,[34] A. B. Morris,[74] A. G. Morris,[55] R. Mountain,[67] H. Mu,[3] F. Muheim,[57] M. Mukherjee,[7] M. Mulder,[47] D. Müller,[47] K. Müller,[49] C. H. Murphy,[62] D. Murray,[61] P. Muzzetto,[26,47] P. Naik,[53] T. Nakada,[48] R. Nandakumar,[56] T. Nanut,[48] I. Nasteva,[2] M. Needham,[57] I. Neri,[20,d] N. Neri,[25,p] S. Neubert,[74] N. Neufeld,[47] R. Newcombe,[60] T. D. Nguyen,[48] C. Nguyen-Mau,[48] E. M. Niel,[11] S. Nieswand,[13] N. Nikitin,[39] N. S. Nolte,[47] C. Nunez,[84] A. Oblakowska-Mucha,[34] V. Obraztsov,[43] D. P. O'Hanlon,[53] R. Oldeman,[26,g] M. E. Olivares,[67] C. J. G. Onderwater,[77] A. Ossowska,[33] J. M. Otalora Goicochea,[2] T. Ovsiannikova,[38] P. Owen,[49] A. Oyanguren,[46,47] B. Pagare,[55] P. R. Pais,[47] T. Pajero,[28,47,o] A. Palano,[18] M. Palutan,[22] Y. Pan,[61] G. Panshin,[82] A. Papanestis,[56] M. Pappagallo,[18,f] L. L. Pappalardo,[20,d] C. Pappenheimer,[64] W. Parker,[65] C. Parkes,[61] C. J. Parkinson,[45] B. Passalacqua,[20] G. Passaleva,[21] A. Pastore,[18] M. Patel,[60] C. Patrignani,[19,b] C. J. Pawley,[78] A. Pearce,[47] A. Pellegrino,[31] M. Pepe Altarelli,[47] S. Perazzini,[19] D. Pereima,[38] P. Perret,[9] K. Petridis,[53] A. Petrolini,[23,a] A. Petrov,[79] S. Petrucci,[57] M. Petruzzo,[25] A. Philippov,[41] L. Pica,[28] M. Piccini,[76] B. Pietrzyk,[8] G. Pietrzyk,[48] M. Pili,[62] D. Pinci,[30] F. Pisani,[47] A. Piucci,[16] Resmi P. K,[10] V. Placinta,[36] J. Plews,[52] M. Plo Casasus,[45] F. Polci,[12] M. Poli Lener,[22] M. Poliakova,[67] A. Poluektov,[10] N. Polukhina,[80,s] I. Polyakov,[67] E. Polycarpo,[2] G. J. Pomery,[53] S. Ponce,[47] D. Popov,[5,47] S. Popov,[41] S. Poslavskii,[43] K. Prasanth,[33] L. Promberger,[47] C. Prouve,[45] V. Pugatch,[51] H. Pullen,[62] G. Punzi,[28,t] W. Qian,[5] J. Qin,[5] R. Quagliani,[12] B. Quintana,[8] N. V. Raab,[17] R. I. Rabadan Trejo,[10] B. Rachwal,[34] J. H. Rademacker,[53] M. Rama,[28] M. Ramos Pernas,[55] M. S. Rangel,[2] F. Ratnikov,[41,81] G. Raven,[32] M. Reboud,[8] F. Redi,[48] F. Reiss,[12] C. Remon Alepuz,[46] Z. Ren,[3] V. Renaudin,[62] R. Ribatti,[28] S. Ricciardi,[56] D. S. Richards,[56] K. Rinnert,[59] P. Robbe,[11] A. Robert,[12] G. Robertson,[57] A. B. Rodrigues,[48] E. Rodrigues,[59] J. A. Rodriguez Lopez,[73] A. Rollings,[62] P. Roloff,[47] V. Romanovskiy,[43] M. Romero Lamas,[45] A. Romero Vidal,[45] J. D. Roth,[84] M. Rotondo,[22] M. S. Rudolph,[67] T. Ruf,[47] J. Ruiz Vidal,[46] A. Ryzhikov,[81] J. Ryzka,[34] J. J. Saborido Silva,[45] N. Sagidova,[37] N. Sahoo,[55] B. Saitta,[26,g] D. Sanchez Gonzalo,[44] C. Sanchez Gras,[31] R. Santacesaria,[30] C. Santamarina Rios,[45] M. Santimaria,[22] E. Santovetti,[29,j] D. Saranin,[80] G. Sarpis,[58] M. Sarpis,[74] A. Sarti,[30] C. Satriano,[30,u] A. Satta,[29] M. Saur,[5] D. Savrina,[38,39] H. Sazak,[9] L. G. Scantlebury Smead,[62] S. Schael,[13] M. Schellenberg,[14] M. Schiller,[58] H. Schindler,[47] M. Schmelling,[15] T. Schmelzer,[14] B. Schmidt,[47] O. Schneider,[48] A. Schopper,[47] M. Schubiger,[31] S. Schulte,[48] M. H. Schune,[11] R. Schwemmer,[47] B. Sciascia,[22] A. Sciubba,[30] S. Sellam,[45] A. Semennikov,[38] M. Senghi Soares,[32] A. Sergi,[52,47] N. Serra,[49] L. Sestini,[27] A. Seuthe,[14] P. Seyfert,[47] D. M. Shangase,[84] M. Shapkin,[43] I. Shchemerov,[80] L. Shchutska,[48] T. Shears,[59] L. Shekhtman,[42,h] Z. Shen,[4] V. Shevchenko,[79] E. B. Shields,[24,e] E. Shmanin,[80] J. D. Shupperd,[67] B. G. Siddi,[20] R. Silva Coutinho,[49] G. Simi,[27] S. Simone,[18,f] I. Skiba,[20,d] N. Skidmore,[74] T. Skwarnicki,[67] M. W. Slater,[52] J. C. Smallwood,[62] J. G. Smeaton,[54] A. Smetkina,[38] E. Smith,[13] M. Smith,[60] A. Snoch,[31] M. Soares,[19] L. Soares Lavra,[9] M. D. Sokoloff,[64] F. J. P. Soler,[58] A. Solovev,[37] I. Solovyev,[37] F. L. Souza De Almeida,[2] B. Souza De Paula,[2] B. Spaan,[14] E. Spadaro Norella,[25,p] P. Spradlin,[58] F. Stagni,[47] M. Stahl,[64] S. Stahl,[47] P. Stefko,[48] O. Steinkamp,[49,80] S. Stemmle,[16] O. Stenyakin,[43] H. Stevens,[14] S. Stone,[67] M. E. Stramaglia,[48] M. Straticiuc,[36] D. Strekalina,[80] S. Strokov,[82] F. Suljik,[62] J. Sun,[26] L. Sun,[72] Y. Sun,[65] P. Svihra,[61] P. N. Swallow,[52] K. Swientek,[34] A. Szabelski,[35] T. Szumlak,[34] M. Szymanski,[47] S. Taneja,[61] F. Teubert,[47] E. Thomas,[47] K. A. Thomson,[59] M. J. Tilley,[60] V. Tisserand,[9] S. T'Jampens,[8] M. Tobin,[6] S. Tolk,[47] L. Tomassetti,[20,d] D. Torres Machado,[1] D. Y. Tou,[12] M. Traill,[58] M. T. Tran,[48] E. Trifonova,[80] C. Trippl,[48] G. Tuci,[28,t] A. Tully,[48] N. Tuning,[31] A. Ukleja,[35] D. J. Unverzagt,[16] A. Usachov,[31] A. Ustyuzhanin,[41,81] U. Uwer,[16] A. Vagner,[82] V. Vagnoni,[19] A. Valassi,[47] G. Valenti,[19] N. Valls Canudas,[44] M. van Beuzekom,[31] H. Van Hecke,[66] E. van Herwijnen,[80] C. B. Van Hulse,[17] M. van Veghel,[77] R. Vazquez Gomez,[45] P. Vazquez Regueiro,[45] C. Vázquez Sierra,[31] S. Vecchi,[20] J. J. Velthuis,[53] M. Veltri,[21,v] A. Venkateswaran,[67] M. Veronesi,[31] M. Vesterinen,[55] D. Vieira,[64] M. Vieites Diaz,[48] H. Viemann,[75] X. Vilasis-Cardona,[83] E. Vilella Figueras,[59] P. Vincent,[12] G. Vitali,[28] A. Vollhardt,[49] D. Vom Bruch,[12] A. Vorobyev,[37] V. Vorobyev,[42,h] N. Voropaev,[37] R. Waldi,[75] J. Walsh,[28] C. Wang,[16] J. Wang,[3] J. Wang,[72] J. Wang,[4] J. Wang,[6] M. Wang,[3] R. Wang,[53] Y. Wang,[7] Z. Wang,[49] H. M. Wark,[59] N. K. Watson,[52] S. G. Weber,[12] D. Websdale,[60] C. Weisser,[63] B. D. C. Westhenry,[53] D. J. White,[61] M. Whitehead,[53] D. Wiedner,[14] G. Wilkinson,[62] M. Wilkinson,[67] I. Williams,[54] M. Williams,[63,68] M. R. J. Williams,[57] F. F. Wilson,[56] W. Wislicki,[35] M. Witek,[33] L. Witola,[16] G. Wormser,[11] S. A. Wotton,[54] H. Wu,[67]

K. Wyllie,[47] Z. Xiang,[5] D. Xiao,[7] Y. Xie,[7] A. Xu,[4] J. Xu,[5] L. Xu,[3] M. Xu,[7] Q. Xu,[5] Z. Xu,[5] Z. Xu,[4] D. Yang,[3] Y. Yang,[5] Z. Yang,[3] Z. Yang,[65] Y. Yao,[67] L. E. Yeomans,[59] H. Yin,[7] J. Yu,[70] X. Yuan,[67] O. Yushchenko,[43] K. A. Zarebski,[52] M. Zavertyaev,[15,s] M. Zdybal,[33] O. Zenaiev,[47] M. Zeng,[3] D. Zhang,[7] L. Zhang,[3] S. Zhang,[4] Y. Zhang,[4] Y. Zhang,[62] A. Zhelezov,[16] Y. Zheng,[5] X. Zhou,[5] Y. Zhou,[5] X. Zhu,[3] V. Zhukov,[13,39] J. B. Zonneveld,[57] S. Zucchelli,[19,b] D. Zuliani,[27] and G. Zunica[61]

(LHCb Collaboration)

[1]*Centro Brasileiro de Pesquisas Físicas (CBPF), Rio de Janeiro, Brazil*
[2]*Universidade Federal do Rio de Janeiro (UFRJ), Rio de Janeiro, Brazil*
[3]*Center for High Energy Physics, Tsinghua University, Beijing, China*
[4]*School of Physics State Key Laboratory of Nuclear Physics and Technology, Peking University, Beijing, China*
[5]*University of Chinese Academy of Sciences, Beijing, China*
[6]*Institute Of High Energy Physics (IHEP), Beijing, China*
[7]*Institute of Particle Physics, Central China Normal University, Wuhan, Hubei, China*
[8]*Univ. Grenoble Alpes, Univ. Savoie Mont Blanc, CNRS, IN2P3-LAPP, Annecy, France*
[9]*Université Clermont Auvergne, CNRS/IN2P3, LPC, Clermont-Ferrand, France*
[10]*Aix Marseille Univ, CNRS/IN2P3, CPPM, Marseille, France*
[11]*Université Paris-Saclay, CNRS/IN2P3, IJCLab, Orsay, France*
[12]*LPNHE, Sorbonne Université, Paris Diderot Sorbonne Paris Cité, CNRS/IN2P3, Paris, France*
[13]*I. Physikalisches Institut, RWTH Aachen University, Aachen, Germany*
[14]*Fakultät Physik, Technische Universität Dortmund, Dortmund, Germany*
[15]*Max-Planck-Institut für Kernphysik (MPIK), Heidelberg, Germany*
[16]*Physikalisches Institut, Ruprecht-Karls-Universität Heidelberg, Heidelberg, Germany*
[17]*School of Physics, University College Dublin, Dublin, Ireland*
[18]*INFN Sezione di Bari, Bari, Italy*
[19]*INFN Sezione di Bologna, Bologna, Italy*
[20]*INFN Sezione di Ferrara, Ferrara, Italy*
[21]*INFN Sezione di Firenze, Firenze, Italy*
[22]*INFN Laboratori Nazionali di Frascati, Frascati, Italy*
[23]*INFN Sezione di Genova, Genova, Italy*
[24]*INFN Sezione di Milano-Bicocca, Milano, Italy*
[25]*INFN Sezione di Milano, Milano, Italy*
[26]*INFN Sezione di Cagliari, Monserrato, Italy*
[27]*Universita degli Studi di Padova, Universita e INFN, Padova, Padova, Italy*
[28]*INFN Sezione di Pisa, Pisa, Italy*
[29]*INFN Sezione di Roma Tor Vergata, Roma, Italy*
[30]*INFN Sezione di Roma La Sapienza, Roma, Italy*
[31]*Nikhef National Institute for Subatomic Physics, Amsterdam, Netherlands*
[32]*Nikhef National Institute for Subatomic Physics and VU University Amsterdam, Amsterdam, Netherlands*
[33]*Henryk Niewodniczanski Institute of Nuclear Physics Polish Academy of Sciences, Kraków, Poland*
[34]*AGH—University of Science and Technology, Faculty of Physics and Applied Computer Science, Kraków, Poland*
[35]*National Center for Nuclear Research (NCBJ), Warsaw, Poland*
[36]*Horia Hulubei National Institute of Physics and Nuclear Engineering, Bucharest-Magurele, Romania*
[37]*Petersburg Nuclear Physics Institute NRC Kurchatov Institute (PNPI NRC KI), Gatchina, Russia*
[38]*Institute of Theoretical and Experimental Physics NRC Kurchatov Institute (ITEP NRC KI), Moscow, Russia*
[39]*Institute of Nuclear Physics, Moscow State University (SINP MSU), Moscow, Russia*
[40]*Institute for Nuclear Research of the Russian Academy of Sciences (INR RAS), Moscow, Russia*
[41]*Yandex School of Data Analysis, Moscow, Russia*
[42]*Budker Institute of Nuclear Physics (SB RAS), Novosibirsk, Russia*
[43]*Institute for High Energy Physics NRC Kurchatov Institute (IHEP NRC KI), Protvino, Russia, Protvino, Russia*
[44]*ICCUB, Universitat de Barcelona, Barcelona, Spain*
[45]*Instituto Galego de Física de Altas Enerxías (IGFAE), Universidade de Santiago de Compostela, Santiago de Compostela, Spain*

[46]*Instituto de Fisica Corpuscular, Centro Mixto Universidad de Valencia—CSIC, Valencia, Spain*
[47]*European Organization for Nuclear Research (CERN), Geneva, Switzerland*
[48]*Institute of Physics, Ecole Polytechnique Fédérale de Lausanne (EPFL), Lausanne, Switzerland*
[49]*Physik-Institut, Universität Zürich, Zürich, Switzerland*
[50]*NSC Kharkiv Institute of Physics and Technology (NSC KIPT), Kharkiv, Ukraine*
[51]*Institute for Nuclear Research of the National Academy of Sciences (KINR), Kyiv, Ukraine*
[52]*University of Birmingham, Birmingham, United Kingdom*
[53]*H.H. Wills Physics Laboratory, University of Bristol, Bristol, United Kingdom*
[54]*Cavendish Laboratory, University of Cambridge, Cambridge, United Kingdom*
[55]*Department of Physics, University of Warwick, Coventry, United Kingdom*
[56]*STFC Rutherford Appleton Laboratory, Didcot, United Kingdom*
[57]*School of Physics and Astronomy, University of Edinburgh, Edinburgh, United Kingdom*
[58]*School of Physics and Astronomy, University of Glasgow, Glasgow, United Kingdom*
[59]*Oliver Lodge Laboratory, University of Liverpool, Liverpool, United Kingdom*
[60]*Imperial College London, London, United Kingdom*
[61]*Department of Physics and Astronomy, University of Manchester, Manchester, United Kingdom*
[62]*Department of Physics, University of Oxford, Oxford, United Kingdom*
[63]*Massachusetts Institute of Technology, Cambridge, Massachusetts, USA*
[64]*University of Cincinnati, Cincinnati, Ohio, USA*
[65]*University of Maryland, College Park, Maryland, USA*
[66]*Los Alamos National Laboratory (LANL), Los Alamos, USA*
[67]*Syracuse University, Syracuse, New York, USA*
[68]*School of Physics and Astronomy, Monash University, Melbourne, Australia*
(associated with Department of Physics, University of Warwick, Coventry, United Kingdom)
[69]*Pontifícia Universidade Católica do Rio de Janeiro (PUC-Rio), Rio de Janeiro, Brazil*
(associated with Universidade Federal do Rio de Janeiro (UFRJ), Rio de Janeiro, Brazil)
[70]*Physics and Micro Electronic College, Hunan University, Changsha City, China*
(associated with Institute of Particle Physics, Central China Normal University, Wuhan, Hubei, China)
[71]*Guangdong Provencial Key Laboratory of Nuclear Science, Institute of Quantum Matter, South China Normal University, Guangzhou, China*
(associated with Center for High Energy Physics, Tsinghua University, Beijing, China)
[72]*School of Physics and Technology, Wuhan University, Wuhan, China*
(associated with Center for High Energy Physics, Tsinghua University, Beijing, China)
[73]*Departamento de Fisica, Universidad Nacional de Colombia, Bogota, Colombia (associated with LPNHE, Sorbonne Université, Paris Diderot Sorbonne Paris Cité, CNRS/IN2P3, Paris, France)*
[74]*Universität Bonn—Helmholtz-Institut für Strahlen und Kernphysik, Bonn, Germany (associated with Physikalisches Institut, Ruprecht-Karls-Universität Heidelberg, Heidelberg, Germany)*
[75]*Institut für Physik, Universität Rostock, Rostock, Germany (associated with Physikalisches Institut, Ruprecht-Karls-Universität Heidelberg, Heidelberg, Germany)*
[76]*INFN Sezione di Perugia, Perugia, Italy*
(associated with INFN Sezione di Ferrara, Ferrara, Italy)
[77]*Van Swinderen Institute, University of Groningen, Groningen, Netherlands*
(associated with Nikhef National Institute for Subatomic Physics, Amsterdam, Netherlands)
[78]*Universiteit Maastricht, Maastricht, Netherlands*
(associated with Nikhef National Institute for Subatomic Physics, Amsterdam, Netherlands)
[79]*National Research Centre Kurchatov Institute, Moscow, Russia (associated with Institute of Theoretical and Experimental Physics NRC Kurchatov Institute (ITEP NRC KI), Moscow, Russia)*
[80]*National University of Science and Technology "MISIS", Moscow, Russia (associated with Institute of Theoretical and Experimental Physics NRC Kurchatov Institute (ITEP NRC KI), Moscow, Russia)*
[81]*National Research University Higher School of Economics, Moscow, Russia*
(associated with Yandex School of Data Analysis, Moscow, Russia)
[82]*National Research Tomsk Polytechnic University, Tomsk, Russia (associated with Institute of Theoretical and Experimental Physics NRC Kurchatov Institute (ITEP NRC KI), Moscow, Russia)*
[83]*DS4DS, La Salle, Universitat Ramon Llull, Barcelona, Spain*
(associated with ICCUB, Universitat de Barcelona, Barcelona, Spain)
[84]*University of Michigan, Ann Arbor, USA*
(associated with Syracuse University, Syracuse, New York, USA)

[a]Also at Università di Genova, Genova, Italy.
[b]Also at Università di Bologna, Bologna, Italy.

[c]Also at Università di Modena e Reggio Emilia, Modena, Italy.
[d]Also at Università di Ferrara, Ferrara, Italy.
[e]Also at Università di Milano Bicocca, Milano, Italy.
[f]Also at Università di Bari, Bari, Italy.
[g]Also at Università di Cagliari, Cagliari, Italy.
[h]Also at Novosibirsk State University, Novosibirsk, Russia.
[i]Also at Laboratoire Leprince-Ringuet, Palaiseau, France.
[j]Also at Università di Roma Tor Vergata, Roma, Italy.
[k]Also at Universidade Federal do Triângulo Mineiro (UFTM), Uberaba-MG, Brazil.
[l]Also at AGH—University of Science and Technology, Faculty of Computer Science, Electronics and Telecommunications, Kraków, Poland.
[m]Also at Università di Siena, Siena, Italy.
[n]Also at Università di Padova, Padova, Italy.
[o]Also at Scuola Normale Superiore, Pisa, Italy.
[p]Also at Università degli Studi di Milano, Milano, Italy.
[q]Also at MSU—Iligan Institute of Technology (MSU-IIT), Iligan, Philippines.
[r]Also at Università di Firenze, Firenze, Italy.
[s]Also at P.N. Lebedev Physical Institute, Russian Academy of Science (LPI RAS), Moscow, Russia.
[t]Also at Università di Pisa, Pisa, Italy.
[u]Also at Università della Basilicata, Potenza, Italy.
[v]Also at Università di Urbino, Urbino, Italy.